UNIVERSIDAD DE INVESTIGACIÓN DE TECNOLOGÍA EXPERIMENTAL YACHAY

Escuela de Ciencias Químicas e Ingeniería

TÍTULO: Characterization of Ecuadorian Clay Pellets for their Potential Adsorption of Hydrogen Sulfide

Trabajo de integración curricular presentado como requisito para la obtención del título de Química

Autor:

Jiménez Mantilla Mayra Alejandra

Tutor:

Ávila Sosa Edward Ebner, PhD.

Co-tutor:

Palma Cando Alex Uriel, PhD.

Urcuquí, Octubre 2020

SECRETARÍA GENERAL
(Vicerrectorado Académico/Cancillería)
ESCUELA DE CIENCIAS QUÍMICAS E INGENIERÍA
CARRERA DE QUÍMICA
ACTA DE DEFENSA No. UITEY-CHE-2020-00060-AD

A los 16 días del mes de octubre de 2020, a las 15:00 horas, de manera virtual mediante videoconferencia, y ante el Tribunal Calificador, integrado por los docentes:

Presidente Tribunal de Defensa	Dra. GONZALEZ VAZQUEZ, GEMA , Ph.D.
Miembro No Tutor	Dr. VILORIA VERA, DARIO ALFREDO , Ph.D.
Tutor	Dr. AVILA SOSA, EDWARD EBNER , Ph.D.

El(la) señor(ita) estudiante JIMENEZ MANTILLA, MAYRA ALEJANDRA, con cédula de identidad No. 1724882178, de la ESCUELA DE CIENCIAS QUÍMICAS E INGENIERÍA, de la Carrera de QUÍMICA, aprobada por el Consejo de Educación Superior (CES), mediante Resolución RPC-SO-39-No.456-2014, realiza a través de videoconferencia, la sustentación de su trabajo de titulación denominado: CHARACTERIZATION OF ECUADORIAN CLAY PELLETS FOR THEIR POTENTIAL ADSORPTION OF HYDROGEN SULFIDE, previa a la obtención del título de QUÍMICO/A.

El citado trabajo de titulación, fue debidamente aprobado por el(los) docente(s):

Tutor	Dr. AVILA SOSA, EDWARD EBNER , Ph.D.
Co - Tutor	Dr. PALMA CANDO, ALEX URIEL , Ph.D.

Y recibió las observaciones de los otros miembros del Tribunal Calificador, las mismas que han sido incorporadas por el(la) estudiante.

Previamente cumplidos los requisitos legales y reglamentarios, el trabajo de titulación fue sustentado por el(la) estudiante y examinado por los miembros del Tribunal Calificador. Escuchada la sustentación del trabajo de titulación a través de videoconferencia, que integró la exposición de el(la) estudiante sobre el contenido de la misma y las preguntas formuladas por los miembros del Tribunal, se califica la sustentación del trabajo de titulación con las siguientes calificaciones:
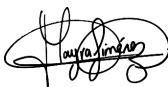
Tipo	Docente	Calificación
Presidente Tribunal De Defensa	Dra. GONZALEZ VAZQUEZ, GEMA , Ph.D.	9,5
Tutor	Dr. AVILA SOSA, EDWARD EBNER , Ph.D.	10,0
Miembro Tribunal De Defensa	Dr. VILORIA VERA, DARIO ALFREDO , Ph.D.	10,0

Lo que da un promedio de: 9.8 (Nueve punto Ocho), sobre 10 (diez), equivalente a: APROBADO

Para constancia de lo actuado, firman los miembros del Tribunal Calificador, el/la estudiante y el/la secretario ad-hoc.

Certifico que *en cumplimiento del Decreto Ejecutivo 1017 de 16 de marzo de 2020, la defensa de trabajo de titulación (o examen de grado modalidad teórico práctica) se realizó vía virtual, por lo que las firmas de los miembros del Tribunal de Defensa de Grado, constan en forma digital.*

JIMENEZ MANTILLA, MAYRA ALEJANDRA
Estudiante

Dra. GONZALEZ VAZQUEZ, GEMA , Ph.D.
Presidente Tribunal de Defensa

Firmado electrónicamente por:
GEMA GONZALEZ

Dr. AVILA   SOSA, EDWARD EBNER , Ph.D.
Tutor

Dr. VILORIA VERA, DARIO ALFREDO , Ph.D.
Miembro No Tutor

CIFUENTES TAFUR, EVELYN CAROLINA
Secretario Ad-hoc
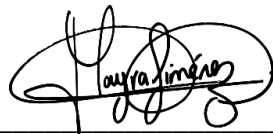
AUTORÍA

Yo, **Mayra Alejandra Jiménez Mantilla**, con cédula de identidad **1724882178**, declaro que las ideas, juicios, valoraciones, interpretaciones, consultas bibliográficas, definiciones y conceptualizaciones expuestas en el presente trabajo; así cómo, los procedimientos y herramientas utilizadas en la investigación, son de absoluta responsabilidad de el/la autora(a) del trabajo de integración curricular. Así mismo, me acojo a los reglamentos internos de la Universidad de Investigación de Tecnología Experimental Yachay.

Urcuquí, octubre 2020.
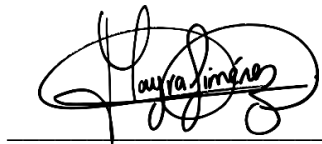
Mayra Alejandra Jiménez Mantilla

CI: 1724882178

AUTORIZACIÓN DE PUBLICACIÓN

Yo, **Mayra Alejandra Jiménez Mantilla**, con cédula de identidad 1724882178, cedo a la Universidad de Tecnología Experimental Yachay, los derechos de publicación de la presente obra, sin que deba haber un reconocimiento económico por este concepto. Declaro además que el texto del presente trabajo de titulación no podrá ser cedido a ninguna empresa editorial para su publicación u otros fines, sin contar previamente con la autorización escrita de la Universidad.

Asimismo, autorizo a la Universidad que realice la digitalización y publicación de este trabajo de integración curricular en el repositorio virtual, de conformidad a lo dispuesto en el Art. 144 de la Ley Orgánica de Educación Superior.

Urcuquí, octubre 2020.

Mayra Alejandra Jiménez Mantilla

CI: 1724882178

Dedication

This thesis is dedicated to my parents, the most important people in my world.

Mayra Alejandra Jiménez Mantilla

Acknowledgments

Resumen

Las arcillas ecuatorianas se propusieron como adsorbente de H_2S, gracias a su alta porosidad y a su área superficial y aparte de esto son abundantes, baratas y amigables con el ambiente. También fueron propuestas debido a la corrosión existente en la industria del gas y del petróleo. El Ecuador cuenta con depósitos no-metálicos los cuales tienen una variedad de minerales pero que no han sido estudiados. Se estudiaron ocho arcillas de tres provincias las cuales tuvieron un tratamiento de secado, extracción de material orgánico, y etiquetado. Luego de este proceso se hicieron pellets a partir de la arcilla con moldes especiales para cada tipo de prueba. Las pruebas mecánicas consistían en investigar la resistencia a la caída libre y la fuerza de compresión de las arcillas. La caracterización de las arcillas se estudió con varias técnicas: Microscopía electrónica de barrido: espectroscopia de rayos X de dispersión de energía (SEM-EDX), infrarrojos por transformada de Fourier (FTIR), análisis termogravimétrico (TGA), fluorescencia de rayos X (XRF), difracción de rayos X en polvo (XRD), fotoelectrones de rayos X Espectroscopia (XPS) y Adsorción y Desorción de N2 con técnica BET y BJH.

Los estudios de SEM-EDX revelaron la presencia de oxígeno (O), silicio, (Si), aluminio (Al), fósforo (P), sodio (Na), nitrógeno (N), y carbono (C) en muestra de arcilla seca y calcinada, pero en la arcilla reaccionada apareció el azufre (S). Los análisis de FTIR mostraron picos que confirmaron la presencia de kaolinita desordenada. Los resultados de XRD mostraron la presencia de cuarzo, kaolinita, guidotita, ortoclasa, muscovita, hematita, sernamontita, titanite, y zircón en estado seco y calcinado de la arcilla, al reaccionar la arcilla presentó dos nuevas fases: kornelita y sulfuro elemental. Los análisis TGA mostraron que la pérdida de masa se debe a hidratación del agua y a la deshidroxilación de las arcillas. Las arcillas calcinadas y secas mostraron isotermas con un perfil similar a la isoterma tipo II con el estudio de adsorción – desorción de nitrógeno. El análisis de XRF mostró Ca, K, Ni, Sr, Ti, Zn y Zr en arcilla seca, calcinada y reaccionada, en esta última se confirmó la aparición de azufre. El análisis XPS mostró las curvas de ajuste de S 2p, O 1s, Si 2p, Al 2p, Fe 2p3, y Cl 2p.

Palabras clave: *Arcillas, sulfuro de hidrógeno, azufre, pellas.*

Abstract

Ecuadorian clays were proposed as an H_2S adsorbent, thanks to the fact that their high porosity and highs surface area as a plus this element is abundant, cheap and environmentally friendly. Also, they are proposed in order to help the corrosion in oil and gas industry. Ecuador has non-metallic deposits which have a variety of minerals. In this work, eight clays from three provinces were studied which had a drying treatment, extraction of organic material, and labeling. After this process, pellets were made from the clay with special molds for each type of test. The mechanical tests consisted of investigating the resistance to free fall and the compression force of the clays. The characterization of the clays was studied with several techniques: Scanning Electron Microscopy – Energy Dispersive X-ray spectroscopy (SEM-EDX), Fourier Transform Infrared (FTIR), Thermogravimetric Analysis (TGA), X-Ray fluorescence (XRF), X-Ray powder Diffraction (XRD), X-Ray Photoelectron Spectroscopy (XPS) and N_2 Adsorption and Desorption.

 SEM-EDX studies revealed the presence of oxygen (O), silicon, (Si), aluminum (Al), phosphorus (P), sodium (Na), nitrogen (N), and carbon (C) at dry and calcined samples. Sulfur (S) appeared only after exposing the pellets to an H_2S atmosphere. FTIR showed peaks that confirmed the presence of disordered kaolinite. The XRD results showed the presence of quartz, kaolinite, guidotite, orthoclase, muscovite, hematite, sernamontite, titanite, and zircon in the dry and calcined state of the clay. After clay reacted, it presented two new phases: kornelite and elemental sulfide. TGA analyzes showed that the mass loss is due to hydration of the water and dehydroxylation of the clays. The calcined and dry clays showed isotherms with a profile similar to the type II isotherm with the nitrogen adsorption-desorption study. The XRF analysis showed the presence of Ca, K, Ni, Sr, Ti, Zn and Zr in dry and calcined pellets, while the presence of sulfur was only observed in reacted clays. XPS analysis for reacted clays showed the fit curves of S 2p, O 1s, Si 2p, Al 2p, Fe 2p3, and Cl 2p.

Keywords: *Clays, hydrogen sulfide, sulfur*, *pellet*

Contents

List of Figures

List of Tables

1. CHAPTER I: INTRODUCTION

Since the 1970s, the oil industry has positioned itself as the economic engine of Ecuador. At the same time that the economy had a strong impulse thanks to this strategic sector, the environmental impact was noticeable in thousands of hectares of the Amazon and the health of the indigenous people who lived in it was deteriorating[1]. Oil extraction includes many polluting processes since the source of the natural gas, once separated from crude oil (if present) it commonly exists in mixtures with other hydrocarbons, principally ethane, propane, butane, and pentanes. In addition, raw natural gas contains among others water vapor, carbon dioxide, helium, nitrogen, and hydrogen sulfide (H_2S) [2]. Currently there are several ways to capture hydrogen sulfide from these mixtures, some examples are: adsorption with the use of natural or synthetic zeolites, activated carbon, metal oxides, etc[3].

The present work proposes using Ecuadorian clays as adsorbent of H_2S because they are abundant, cheap, and environmentally friendly and due to their high porosity and highs surface area. In Ecuador, there are deposits of them that have not been adequately investigated to obtain geological and chemical information that helps the industry in their economic activity. Each clay deposit can contain a variety of minerals that drastically change the clays' chemical and physical properties. In our country, the clay deposits can be ubicated in Azuay, Zamora Chinchipe, and Morona Santiago Provinces. The clays used for this work come from these provinces. Then, clay pellets were prepared as solid-beds. On these pellets were carried out mechanical and reactivity tests in the chemistry and geology laboratories of the Yachay Tech University. Further characterization was carried out in collaboration with the Catholic University of Peru and the Center for Research in Applied Science and Advanced Technology (CICATA), a standard unit that is part of the Polytechnic Institute of Mexico (IPN).

Chapter II shows concepts that support this work, including the oil in Ecuador, natural gas, hydrogen sulfide, clays, and the characterization methods used in this work. Chapters III and IV show the problem and the objectives of this work. Chapter V indicates in detail the line of action from the work of collecting samples to then go on to a physical test, which was implemented to select the clays most resistant to impact. And it ends with an explanation of each characterization technique used. In Chapter VI, the results, each characterization process through which the clay passed to determine the morphology, the chemical and elemental composition, the pore volume,

and the external surface are explained. The reactivity tests for this type of clays is proposed. Finally, Chapter VII shows the conclusions of this work.

2. CHAPTER II: LITERATURE REVIEW

2.1. Petroleum in Ecuador

Ecuador is one of Latin America's largest oil exporters, with net oil exports estimated at 285,000 barrels per day (bbl/d) in 2010. The oil sector accounts for about 50 percent of Ecuador's export earnings and about one-third of all tax revenues. Despite being an oil exporter, Ecuador must still import refined petroleum products due to the lack of sufficient domestic refining capacity to meet local demand. As a result, the country does not always enjoy the full benefits of high world oil prices: while these high prices bring Ecuador greater export revenues, they also increase the country's refined product import bill[4].

According to the report of the Central Bank of Ecuador in the fourth quarter of 2019, the production of Petroamazonas EP was 37.82 million barrels, with an average daily production of 411.13 thousand barrels, which represents 5.1% less than the average daily production in relation to the previous quarter and an increase of 2.3% compared to the fourth quarter of 2018. Between January and December 2019, the income from internal sales of diesel, high octane naphtha and LPG was USD 2,583.29 million, while the cost of its import reached USD 3,816.05 million[5].

2.2. Corrosion in oil and gas industry

Corrosion encountered in the production of oil and gas is very costly and it involves direct and indirect costs associated with lost time, the replacement of materials of construction, and the continuous involvement of personnel in corrosion management as well as safety and environmental consequences. In 2016, NACE International released the "International Measures of Prevention, Application and Economics of Corrosion Technology (IMPACT)" study, which estimates the global cost of corrosion to be approximately US$2.5 trillion. The study reviewed cost of corrosion studies performed by several countries including, Australia, China, Finland, Germany, India, Japan, Kuwait, Sweden, the United Kingdom, and the United States. Based on these studies, the annual corrosion costs in each nation ranged from approximately 1–5% of their gross national product (GNP). These studies do not include the cost of corrosion failures consequences on safety and environment. The IMPACT study found that significant savings between 15% and 35% of the cost of damage can be realized by implementing corrosion control practices that are equivalent to reducing the global corrosion cost by US$375–875 billion annually[6].

2.3. Clay deposits in Ecuador

The inventory of non-metallic raw materials determined the presence of important mineral deposits in all the provinces of Ecuador. In relation to clay minerals, it was determined that their occurrence represents on average around 20% of the country's Non-metallic mineral wealth.

Regarding the use of the valued clay mineral wealth, it was evidenced that about 50% of it is dedicated to the traditional (artisan) manufacture of bricks and tiles that satisfy the local demand of the provinces. Only approximately 15% of the clay mineral wealth is used by the industrial sector producing fine ceramics; the rest are in the phase of determining the feasibility of use and application in the ceramic sector, which indicates the untapped clay mining potential of the country. It is confirmed that Ecuador has important non-metallic resources, which must be used for its integral development[7].

2.4. Crude Oil

Crude oil is a complex mixture consisting of 200 or more different organic compounds, mostly alkenes (single bond hydrocarbons on the form CnH_{2n+2}) and smaller fraction aromatics (six-ring molecules such as benzene C_6H_6). Different crude contains different combinations and concentrations of these various compounds. The API (American Petroleum Institute) gravity of a particular crude is merely a measure of its specific gravity, or density. The higher the API number expressed as degrees API, the less dense (lighter, thinner) the crude. This means, put simply, that the lower the degrees API, the denser (heavier, thicker) the crude. Crude from different fields and from different formations within a field can be similar in composition or be significantly different. In addition to API grade and hydrocarbons, crude is characterized for other undesired elements like sulfur among others which is regulated and needs to be removed. Crude oil API gravities typically range from 7 to 52 corresponding to about 970 kg/m^3, but most fall in the 20 to 45 API gravity range. Although light crude (i.e. 40-45 degrees API, it contains shorter molecules, which means a lower carbon number. This also means it contains less of the molecules useful as high octane gasoline and diesel fuel, the production of which most refiners try to maximize. If a crude is heavier than 35 degree API, it contains longer and bigger molecules that are not useful as high octane gasoline and diesel fuel without further processing. [2]

2.5. Natural Gas

Natural gas that comes from oils wells is typically termed "associated gas". This gas can exist separate from oil in the formation (free gas), or dissolved in the crude oil (dissolved gas). Natural

gas from gas and condensate wells, in which there is little or no crude oil, is termed 'non-associated gas'.

Gas wells typically produce dry natural gas only. However condensate wells produce free natural gas along with a semi-liquid hydrocarbon condensate. Whatever the source of the natural gas, once separated from crude oil (if present) it commonly exists in mixtures with other hydrocarbons, principally ethane, propane, butane, and pentanes. In addition, dry natural gas contains water vapor, hydrogen sulfide (H_2S), carbon dioxide, helium, nitrogen, and other compounds. [2]

2.6. Hydrogen Sulfide

Almost all the chemicals are hazardous and toxic when it is exposed to the human body. Out of these chemicals, hydrogen sulfide, is a colorless gas with a bad odor of rotten eggs. It is highly toxic, corrosive and flammable (See Table 1). Sewer gas is dangerous as a toxic gas at low concentrations and as a highly combustible gas. It is commonly found in natural sources and can be released with commercial methods.

Table 1 Physical and Chemical Properties of hydrogen sulfide.

Property	Value	Unity
Molar mass	34.081	g/mol
Specific gravity	1.2	-
Lower explosive limit (LEL)	4.5	%
Upper explosive limit (UEL)	46	%
Normal boiling point	212.9	K
Melting point	190.9	K
Critical temperature	373.4	K
Auto ignition temperature	206	°C
Critical pressure	89.7	bar
Critical density	0.349	g/cm^3
Kinetic diameter	3.6	Å
Dipole moment	0.97	D
Odor	rotten eggs	-
Appearance	colorless gas	-
Threshold limit value (TLV)	1	ppm
Immediate danger limit	100	ppm

2.6.1. Human Health Effects

In petroleum industry the toxic exposure of hydrogen sulfide is higher than in other industries and is responsible for many health incidents, H_2S is a common and potent toxic agent that is the primary chemical hazard of sour gas production.[8]

Therefore, one should not fully trust their sense of smell for the presence of H_2S because alarming concentrations may be present with no perceivable odor.

Hydrogen sulfide is both an irritant and a chemical asphyxiant with effects on both oxygen utilization and the central nervous system. Its health effects can vary depending on the level and duration of exposure.[9]

The effects be determined by on the level exposure of H_2S. It can vary from an odor threshold, nausea, tearing eyes, eyes irritation, and lung irritation, olfactory paralysis until sense of smell paralyzed, pulmonary edema, and amnesia for time of exposure among others. All these effects depend directly of the quantity of ppm of H_2S and the time exposed directly to the human body[10].

No antidote is currently available for sulfide poisoning and treatment is largely supportive.

2.6.2. Toxicology

Hydrogen sulfide is a highly toxic gas—second only to carbon monoxide as a cause of inhalational deaths. Its mechanism of toxicity is only partially known, and no specific therapy exists for sulfide poisoning.[11]

Concentration is much more important than duration of exposure. Compared to other inhaled toxic substances, hydrogen sulfide gives little margin of safety. Fatal exposures to hydrogen sulfide in humans, for example, in theory may take place at 150 ppm for 6 hours (concentration x time product = 0.252) or 650 ppm for 8.5 minutes (0.005). This means that, for hydrogen sulfide, higher concentrations are much more toxic, even with proportionally shorter exposure levels, for both mortality and experimental pulmonary edema induced in the rat. [12]

In toxicology, a syndrome that is associated with a particular poison is called a ''toxidrome.'' In contrast, hydrogen sulfide toxicity is one of the most unusual and reliable toxidromes in medical toxicology (and clinical medicine in general).[12]

- ''Knockdown'' (acute central neurotoxicity)
- Pulmonary edema
- Conjunctivitis

- Odor perception followed by olfactory paralysis

2.7. Technologies of capture of hydrogen sulfide

The hydrogen sulfide composition in biogas ranges from 0-5 % depending on the feed source to the biogas digester. Liquid phase chemical scrubbing with amines is one of the major acid gas removal techniques. Adsorption on solid materials, on the other hand, is a potentially more energy-efficient technique for both CO_2 and H_2S capture. Hydrogen sulfide removal is a long-standing economic and environmental challenge faced by the oil and gas industries. H_2S separation processes using reactive and non-reactive absorption and adsorption, membranes, and cryogenic distillation. Sour gas contains significantly amounts of hydrogen sulfide[3].

2.8. Clays

The term **"clay"** refers to a naturally occurring material composed primarily of fine-grained minerals, which is generally plastic at appropriate water contents and will harden when dried or fired. Clay usually contains phyllosilicates, it may contain other materials that impart plasticity and harden when dried or fired. Associated phases in clay may include materials that not impart plasticity and organic matter[13]

2.8.1. Classification

Kaolinite: This clay mineral is the weathering product of feldspars. It has a white, powdery appearance. Kaolinite is named after a locality in China called Kaolin, which invented porcelain (known as china) using the local clay mineral. The ceramics industry uses it extensively. Because kaolinite is electrically balanced, its ability of adsorb ions is less than that of other clay minerals.

Smectite: This clay mineral is the weathering product of mafic silicates, and is stable in arid, semi-arid, or temperate climates. It was formerly known as *montmorillonite*. Smectite has the ability to adsorb large amounts of water, forming a water-tight barrier. It is used extensively in the oil drilling industry, civil and environmental engineering (where it is known as bentonite), and the chemical industry.

Illite: Resembles muscovite in mineral composition, only finer-grained. It is the weathering product of feldspars and felsic silicates. It is named after the state of Illinois, and is the dominant clay mineral in mid-western soils.

Chlorite: This clay mineral is the weathering product of mafic silicates and is stable in cool, dry, or temperate climates. It occurs along with illite in mid-western soils. It is also found in some metamorphic rocks, such as chlorite schist.

Vermiculite: This clay mineral has the ability to adsorb water, but not repeatedly. It is used as a soil additive for retaining moisture in potted plants, and as a protective material for shipping packages.

Palygorskite (attapulgite)**:** Palygorskite is synonymous terms for the same hydrated Mg-Al silicate material. This mineral actually resembles the amphiboles more than it does clay minerals, but has a special property that smectite lacks - as a drilling fluid, it stable in salt water environments. When drilling for offshore oil, conventional drilling mud falls apart in the presence of salt water. Palygorskite is used as a drilling mud in these instances[13].

2.8.2. Physical and Chemical Properties

The physical and chemical properties of particular clay and clay minerals are dependent on the structure and composition. The structure and composition of the major industrial clays, i.e. kaolins, smectites, illite and palygorskite-sepiolite , are very different even though each is comprised of octahedral and tetrahedral sheets as their basic building block. However, the arrangement and composition of the octahedral tetrahedral sheets account for most differences in their physical and chemical properties, and can even affect characteristics as particle size and porosity.

2.9. Types of characterization

Various techniques were used to determine the morphology, the chemical and elemental composition, the pore volume and the external surface area as shown in the following table:

Table 2 Techniques used in the characterization of Ecuadorian clays.

Techniques*	Purpose
Scanning Electron Microscopy – Energy Dispersive X-ray spectroscopy (SEM-EDX)	Affords a magnified 3D view of clay surface with great depth of focus. Identify the elements and clay's concentration.
Fourier Transform Infrared (FTIR)	Identify chemical bonds present in the clays.
Thermogravimetric Analysis (TGA)	Quantify the mass loss at a determine range of temperature.
X-Ray fluorescence (XRF)	Determine the chemical composition.
X-Ray powder Diffraction (XRD)	Determine the morphological composition.
X-Ray Photoelectron Spectroscopy (XPS)	Quantitative determination and identification of chemical states.
N_2 Adsorption and Desorption with BET and BJH technique.	Determine the total specific surface area, pore area and specific pore volume.

* For the fundamentals of these characterization techniques, see Annex 1.

3. CHAPTER III: PROBLEM STATEMENT

Oil extraction releases natural gases such as hydrogen sulfide, one of the most toxic gases for humans and also this gases For this reason, it is essential to remove it from the natural gas composition. There are several technologies to the gas sweetening process, such as chemical solvents, physical solvents, membranes, and adsorption with solid beds. The use of solid beds consists of transforming sour gas into sweet gas by a contact tower.

The solid bed is constituted by different type of material and this work seeks to use an economical and environmentally friendly solution, such as clay, which would be extracted from the natural/non-metallic deposits of Ecuador. The clays have been collected from three provinces Azuay, Zamora Chinchipe, and Morona Santiago. The use of clay pellets is considered a potential type of hydrogen sulfide adsorbent in solid bed, depending on their minerals and morphological characteristics. The following steps are followed to optimize our clay pellets for H_2S capture: sampling, labeling, remove moisture, pellets molding, calcination, mechanical tests, reactivity and characterization techniques (SEM-EDX, FTIR, TGA, XRF, XRD, XPS, N_2 adsorption and desorption test).

4. CHAPTER IV: OBJECTIVES

4.1. General Objective

To choose the best clay among eight clays collected at Azuay, Zamora Chinchipe, and Morona Santiago to generate clay pellets for the capture of hydrogen sulfide.

4.2. Specific Objective

To create hand-made pellets and calcined them for the next tests.

To choose the best clay with tests of resistance to drop, porosity and uniaxial compression.

To determine the morphology of the clays using microscopy analysis such as SEM.

To use FTIR technique to Identify chemical bonds present in the clays.

To determine mass loss up to 500 °C using thermal analysis like TGA.

To determine surface area, pore volume using nitrogen adsorption - desorption analysis technique.

To use spectroscopy analysis such as EDX, XRF, and to determine the elemental composition of the clays.

To analyze the mineralogical composition of the clays using the X-ray powder diffraction technique.

To determine chemical environment and elemental composition on the surface the technique XPS was required.

5. CHAPTER V: METHODOLOGY

5.1. Sampling location description

Fresh clay samples were collected by the Research Group Applied in Materials and Processes (GIAMP) from the southern of Ecuador, specifically, Zamora Chinchipe which is a province located in the south-east of the Ecuadorian Amazon and from Morona Santiago which is located in the southern center of the country, in the geographical area known as the Amazon region. And each sample comes from a different county and has a code to differentiate between them. The clays were received and labeled. Then they went on to the drying process of the sample in an oven at 60 °C for 5 hours.
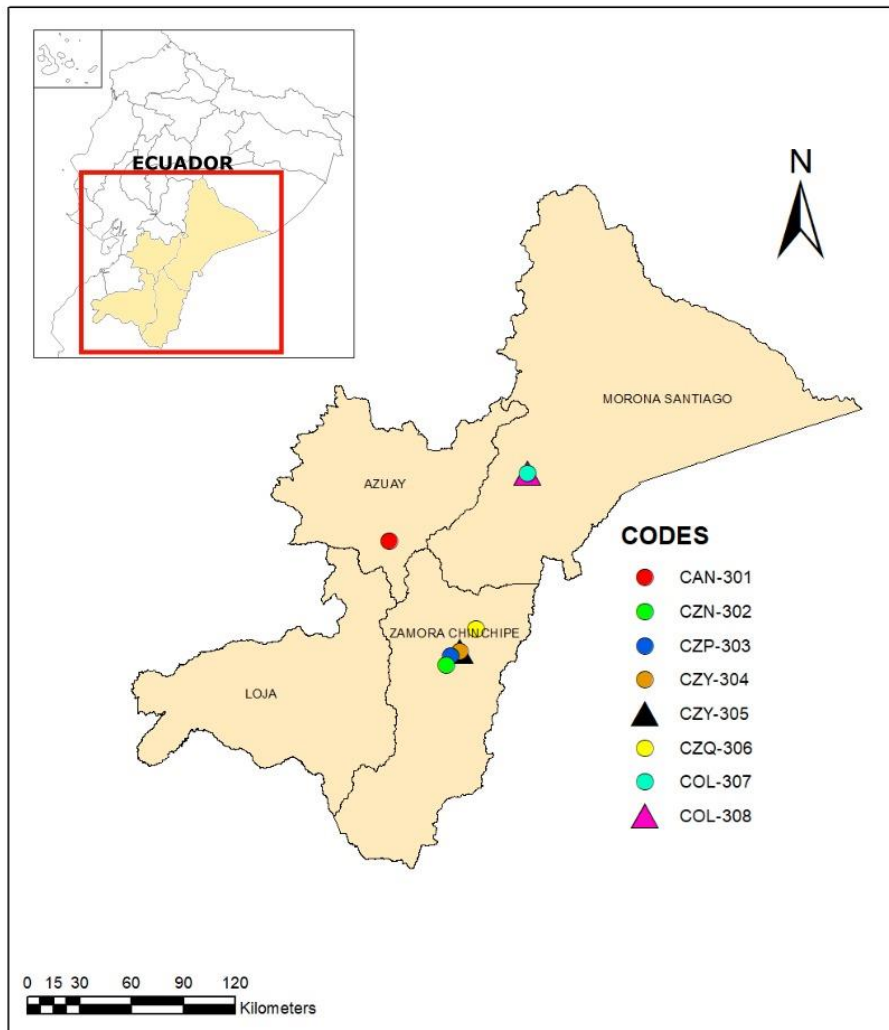
Figure 1 Location map of the study area in Ecuador.

5.2. Labeling of samples

Labeling of clays samples consisted of a code of three letters and three numbers for each of them. The first letter, **C**, is for Clay; the second one belongs to the province codification according to this, **A** refers to Azuay, **Z** refers to Zamora Chinchipe and **O** refers to Morona Santiago. Then the third one indicates the place where the sample was picked up, so **N** refers to Nabon, **Y** refers to Yanzatza, **P** refers to Panguintza, **Q** refers to Quiringe and **L** refers to Limon Indanza. Finally the first number shows the sampling campaign, and the next two numbers correspond to sample collected in each trip.

Table 3 Clay samples with their location description.

CODE	SAMPLE	Location	UTM Coordinates	
			Latitude	Longitude
180807.1	CAN-301	10 Km South of the Nabon canton crossing with the Cuenca-Loja panamericana highway, Azuay province.	-3° 18' 33.28" S	-79°08' 20.89" W
180807.3	CZN-302	1 Km to the North of the bridge on the Namirez river, between Cumbaratza to the South and La Saquea to the North, Zamora province	3° 57' 16.73" S	78° 50' 43.05" W
180808.5	CZP-303	0.2 Km SW of Panguintza, courve, North of the La Saquea, Zamora province	3° 54' 18.08" S	78° 49' 09.16" W
180807.6a	CZY-304	10Km South of Yanzatza canton, North of Panguintza county, Zamora province.	3° 52' 50.39" S	78° 46' 28.48" W
180807.6b	CZY-305	10Km South of Yanzatza canton, North of Panguintza county, Zamora province.	3° 52' 50.39" S	78° 46' 28.48" W
180807.8	CZQ-306	Quiringue community, North of La Yona county, North of the bridge on the Chicaña river, Zamora province.	3° 45' 43.58" South	78° 41' 28.48" W
180808.8a	COL-307	North of Limon Indanza canton, Morona-Santiago province.	2° 57' 03.49" South	78° 25' 18.70" W

5.3. Work methodology

The research was carried out using eight natural clays to pass four stages:

i.   Clays pellets preparation and molded.

ii.   Physical tests that include tests of clay resistance and porosity.

iii. The second stage, reactivity, in which the clay is placed in an environment that recreates the presence of acid gases and how it adsorbs them.

iv.   Characterization. In the final stage the clay that obtained the best reactivity results chosen to determine the type of minerals present in the clay.

5.3.1.   Clay pellets preparation and molded

The clay was mixed with enough water to create a clay-like dough, then placed in the drying oven (SLN 115 POL-EKO-APARATURA) at 60 °C for approximately 15 minutes to remove excess moisture. Then it was put in the muffle "Vulcan A550" for 14 hours at a temperature of 450 ° C to obtain a medium calcination process.

The clay pellets were hand-made with custom-made molds. The spheres had a diameter of 13 mm as it shown in Figure 2 a, b, cylinders had a diameter of 13 mm and a height of 26 mm Figure 2 c to maintain the 2:1 ratio according to the 'ASTM D2166' standard. The two types of pellets were used for different types of mechanical tests and chemical tests.
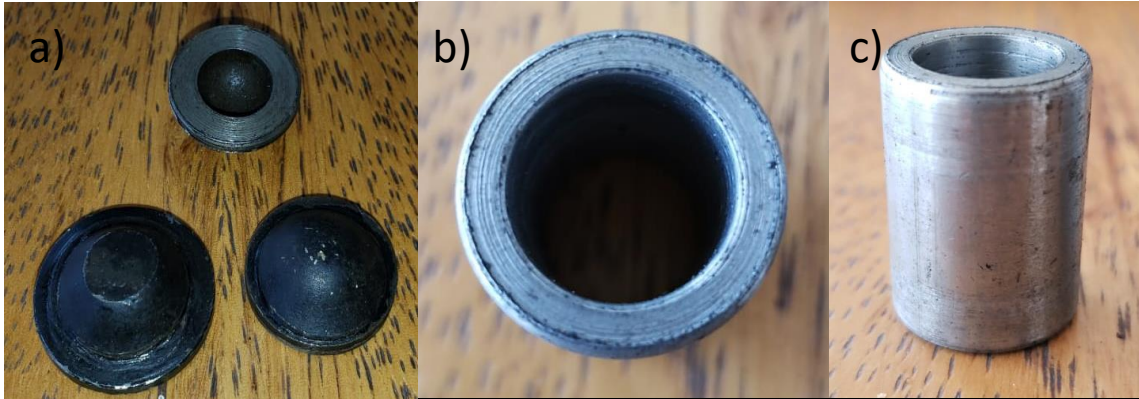
Figure 2 Molds to make pellets (a), (b) spheres and (c) cylinders of clay.

Figure 3 a) Muffle Vulcan A-550 b) Clay samples before calcination process.

5.3.2. Mechanical Testing

5.3.2.1. Free-fall-drop impact test

For this test were used the sphere pellets. Each one of the pellets were positioned at a height of 1.50 m and drooped on a ceramic surface, a camera was used to record the number of rebounds and their height. The number of possible drops before the breakout was noted. The free-fall test was performed with at least seven pellets for each sample.

Figure 4 Free-fall drop test at 1.50m of height.

5.3.2.2.   Uniaxial compression test

The cylindrical sample was prepared in a way that it could be attached to the sage of the microCT-BRUKER Type: MTS3. The compression was then measured at a constant speed of 10.9, on three trials were used for this test and the machine gave diagrams of force (N) versus deformation (mm) with which it was possible to perform compression strength and loading force results. The software used in this test was: Mts.

Figure 5 Bruker microCT Type: MTS3.

5.3.2.3. Porosity test by 3D nanotomography

The sample was scanned using X-ray micro-computed tomography, SkyScan 2211 Multiscale CT (see Figure 6). After acquisition of the slice images, the data are reconstructed into a 3D volume. This can be summarized into four tasks: (1) realigning the images; (2) correcting for instrument based artefacts; (3) segmentation; and (4) visualization[14]. This technique shows the closed and open pores of the material and their connections. We are using CTVox and NRecon software's for 3D visualization[15].
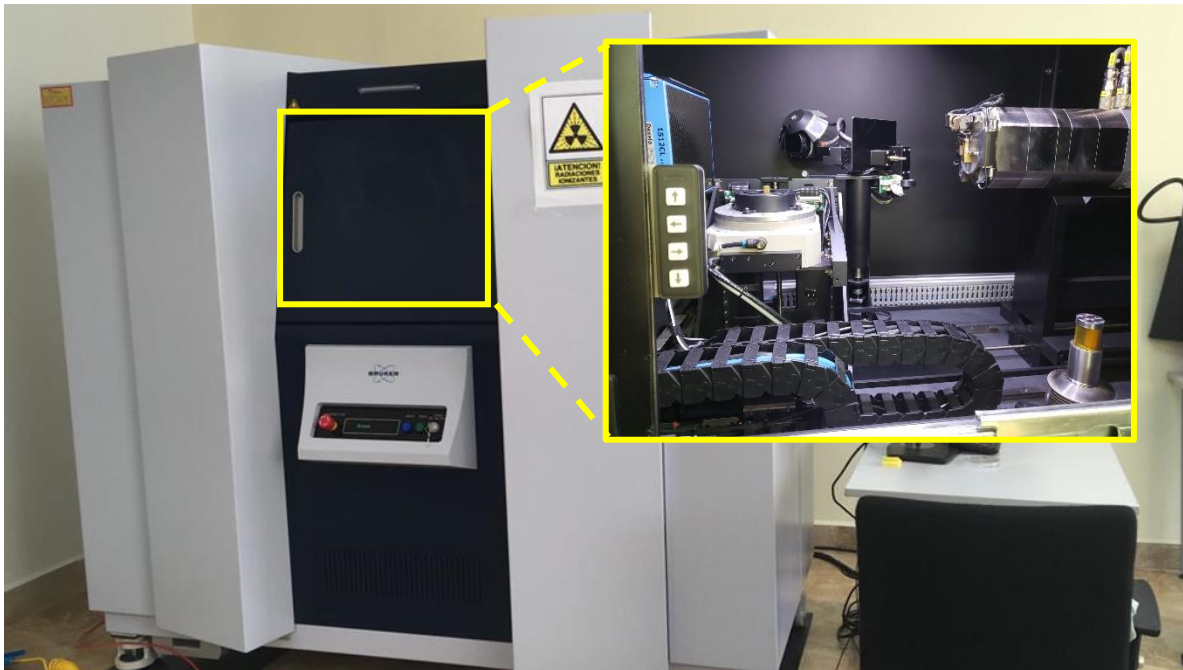
Figure 6 MULTISCALE X-ray nanotomography SKYSCAN 2211.

5.3.2.4.　Porosity Test by volumen difference

For this experiment, four types of clays calcined at 450 °C were used, as explained in section 4.3.1, the dimensions of the clay (height and diameter) were taken, then clean and dry sample was weighed on an analytical balance with a precision of four decimals. Then they were left for 6 days in 250 ml beakers with 200 ml of water, the samples were suspended with a thread to avoid contact with the walls of the beakers. The sample is then removed from the beakers and the excess saturating liquid is removed with the fingers and the saturated sample is quickly weighed and the porosity is calculated according to:

$$Volume = \frac{dry\ weight - satured\ weight}{density\ of\ liquid}$$

5.4. Chemical Testing

5.4.1.　Reactivity

Warning: The use of a special mask for hydrogen sulfide, goggles and gloves is mandatory to carry out the following experiment. For reactive test was verified that the glassware is completely clean and dry. 1.0 g of FeS were weighed and then was placed into the test tube, (this step was

done with caution to avoid pouring it on the walls of the tube. The, the test tube was placed inside a balloon. After that, the balloon was covered very carefully and tightly with a septum, then with the help of then with the help of a previously sweetened needle was added 2 ml of hydrochloric acid into the test tube (avoid falling out of the test tube). The reaction is allowed to rest for a week.

Table 4 Materials and reagents of reactive test

Materials	Reagents	
	Name	CAS
Round bottom flask	Ferrous Sulfide (FeS)	1317-37-9
Glass rod	Hydrochloric acid (HCl)	7647-14-5
Test tube	Sodium Hydroxide (NaOH)	2815 12 00
Beaker		
Syringe		
Spatula		
Pipette		
Septum		
Gloves		
Safety goggles		
Mask (H$_2$S respirator)		
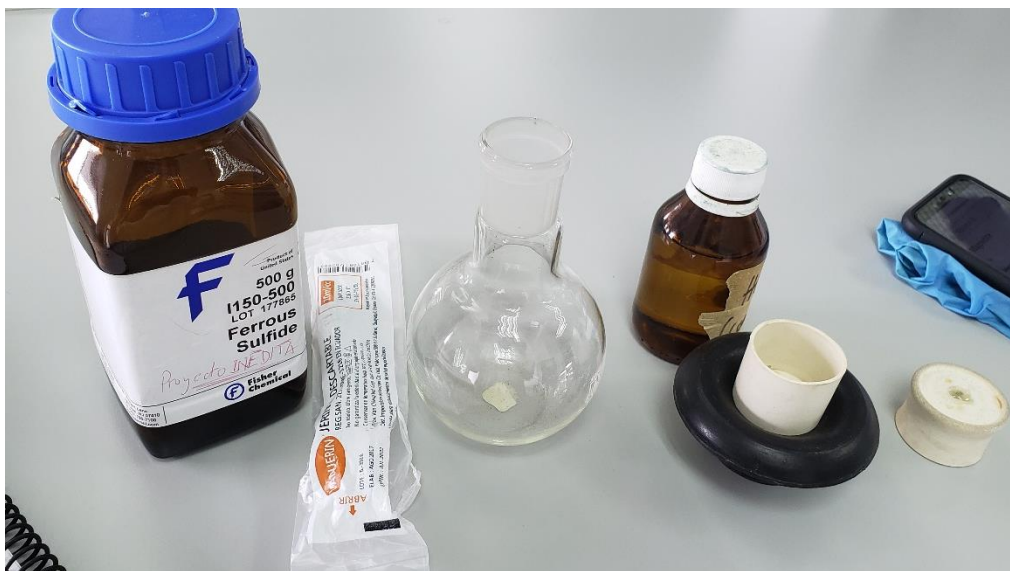
Figure 7 Materials used for reactivity test.

Figure 8 Assemble of FeS + HCl reaction with clay sample

To disassemble the reaction, prepare a 35 % NaOH solution. With a new needle remove the gases created during the reaction and pour them into the NaOH preparation. After performing the process between 10 - 20 times, the septum can be removed and the reacted pellet removed, it must be left in a drying chamber.

5.5. Characterization Techniques

5.5.1. Fourier-transform infrared Spectroscopy

Dry and calcined powder samples were place into a conventional 13 mm diameter disk under 60 kN of pressure for 1 minute. For the data spectrum collecting was done in ART-IR scanning mode with a Spectrum One spectrometer, from Perkin-Elmer (see **Figure 9** *Perkin Elmer Spectrum One*Figure 9).

Figure 9 Perkin Elmer Spectrum One

5.5.2. Scanning Electron Microscope

The calcined and reacted with 0.5 g and 1.0 g of FeS samples were cut in half and thanks to this the adsorption layers were observed for microstructural analysis. For the micrograph measurement on the equipment Phenom Pro X (see

Figure **10**), and they were taken with a backscatter electrons (image contrast composition detector) working at 15 keV. The elemental analysis was measured by EDX detector with a FAST SDD from AMPTEK, and the process data was performed with PHENOM PROSUITE software.

Figure 10 Phenom ProX scanning electron microscope.

Figure 11 Raw, Reacted and Calcined (from left to right) clay of CZY-304 sample.

5.5.3. X-Ray Diffraction

The dry, calcined and reacted samples which were pulverized for optimal analysis. X-ray powder diffraction data were collected in a D8 Discover with DaVinci diffractometer from Bruker, equipped with a Cu tube, (CuKα radiation) and a Lynx-eye of detector. The data collected were done in a range of $5º \leq 2\theta \leq 69º$ in steps of $0.02º$ with an integration time per step of 0.3s. The crystalline phase's analysis was achieved in two part as describes bellow:

5.5.3.1. Crystalline phases identification

The crystalline phase's identification is very important in the solid materials characterization because they depend on your mechanical, physical, and chemical properties. Currently, this step was carried out utilizing Qualx 2.8[16] and SmartLab Studio 4.3 software[17]. In both cases, the crystallography open database (COD)[18,19] was used as the powder diffraction patterns database. The data reduction (the smoothing, background and zero-point corrections, and peak search) of powders diffraction was done with each one software. In this case, it is employed to apply search-

match methodology[20] and to obtain the list of crystalline phase candidates possible as constituents of the clays.

5.5.3.2. Crystalline phases quantification

The whole powder pattern fitting (WPPF) methodology was implemented by Toraya[21,22] in 90´s decade. This methodology has been shown that is one alternative technique for the crystalline phase quantitation in the natural different materials: for example, the clays. In this work, it was applied for crystalline phase quantitation to find the relative abundance of the crystalline phases presents in the clays by using SmartLab Studio 4.3 software[17].

5.5.4. X-Ray Fluorescence Spectroscopy

The XRF analyses were carried out using a portable Bruker AXS Tracer III-SD instrument equipped with a rhodium X-ray tube and a Si-PIN detector. Instrument's voltage and current were set to 40kV and 10.3 µA. No radiation filters were used. Measuring time was set to 60s. XRF spectra were analyzed using the software Spectra 7.4.0 from Bruker AXS. Data were collected on manually compressed powdered samples.

5.5.5. X-Ray Photoelectron Spectroscopy

The equipment used for this experiment was: X-Ray Photoelectron Spectroscopy (XPS) PHI VersaProbe III (Physical-Electronics) equipped with a 180 hemispherical electron energy analyzer and excited by a monochromatized Al-K source with an energy 1486.6 eV. Its energy analyzer operates in the pass energy mode at 280 eV for Survey and 55 eV for high resolution.

Figure 12 X-Ray Photoelectron Spectroscopy VersaProbe III.

5.5.6. Thermal Gravimetric Analysis

Thermogravimetric analysis (TGA) of clay were obtained in Q5000 IR furnace (See Figure 13) the samples were loaded automatically in the thermal analyzer and heated at 10 °C/min. The conditions used in the measurements of the dry clays are: ramp speed of 10.00 °C/min, the sample gas is air, and the temperature range is 40 - 500 °C. Weighing accuracy ± 0.1%. Sensitivity <0.1 pg.

Figure 13 Q5000 IR Thermogravimetric Analyzer.

Figure 14 Placing the sample in the TA.

5.5.7. Nitrogen adsorption-desorption analysis

The raw sample was weighed directly into powder, unlike the wet sample, which when calcined, an agate mortar was used to break up the sample and obtain small pieces for analysis. Analyses were obtained with a Micromeritics' ASAP 2050 Xtended Pressure Sorption Analyzer (See Figure 15). The adsorption properties of the adsorbent, in this case, the clay, were degassed at 120 °C for 5 h prior to the measurement at 75 K, approximately.

The clays were studied at raw and calcined form with the following conditions:

Table 5 Parameters for adsorption properties.

Parameters	Dry Clay	Calcined Clay
Analysis Adsorptive	N2	N2
Analysis Bath Temperature	75.205 K	75.431 K
Sample mass	0.0457 g	0.0470 g
Equilibration Interval	50 s	50 s
Ambient Temperature	22.00 °C	22.00 °C
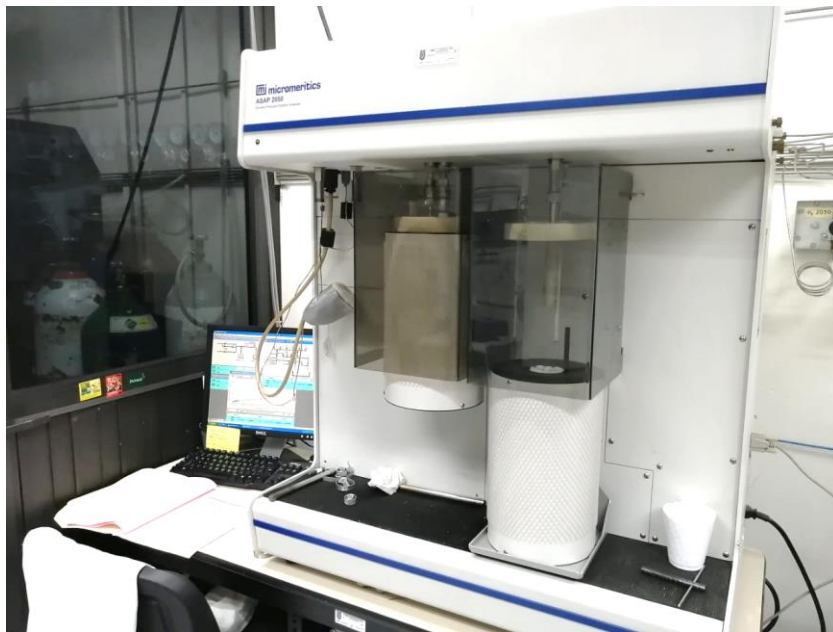
Figure 15 Micromeritics' ASAP 2050 Xtended Pressure Sorption Analyzer.

6. CHAPTER VI: RESULTS AND DISCUSSION

6.1. Physical Testing

6.1.1. Free fall-drop impact test

This method is used to evaluate the ability of pellets to resist a free fall impact and to compare the best performance of different pellet designs. The first test was carried out with the eight clays with a diameter of 9 mm described in Table 3. As can be seen in Figure 16a, the average to they looked for a better resistance in the samples CZY-304, CZY -305, CZQ-306 and COL-307 with an average of six falls without breaking, instead, the remaining clays broke on the first impact and the main idea is the study of a single clay for use as adsorption of acid gases, from this, it is decided to use the clay that shows the best results in resistance tests.
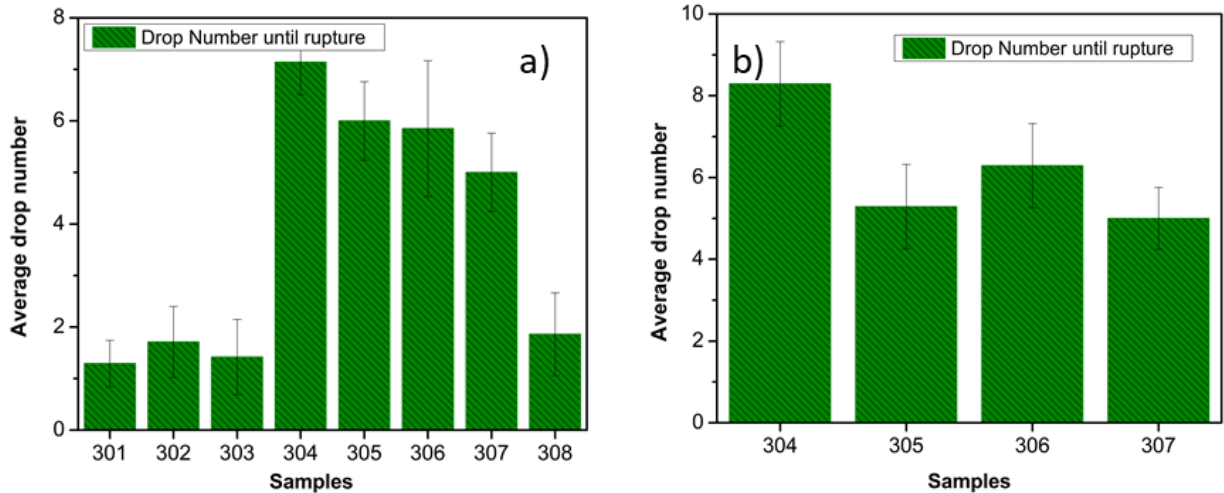
Figure 16 Free fall drop impact test with eight clays with diameter of 9mm (a) and with four clays with diameter of 13 mm (b).

Four clays are eliminated from the drop test for the following resistance and characterization studies. In Figure 16.b the test was carried out with the best four clays from the first test, but in this occasion the diameter of the pellets were 13 mm. The sample CZY-304 shows a better behavior in the resistance test with an average greater than eight falls before its break, but its companions follow the same behavior with an average greater than five falls before the break, so it is decided to continue with uniaxial compression tests to have more reference data.

6.1.2. Uniaxial compression test

The requirements of the pellets in an acid gas adsorption tower includes a standard in the packing of solid bed packing during adsorption process; at this point, it is seek to avoid the breaking of the pellets and free fall experiments were carried out for this point. Besides, the uniaxial compression test is used to compare clays calcined at 450 °C and moistened after being calcined. Since the free-fall drop impact test was not enough to determine a single clay, the best four clays from the previous experiment are studied to have more choice variables.

It was proposed that perhaps a new phase was created due to the remarkable difference between calcined and wetted clays.
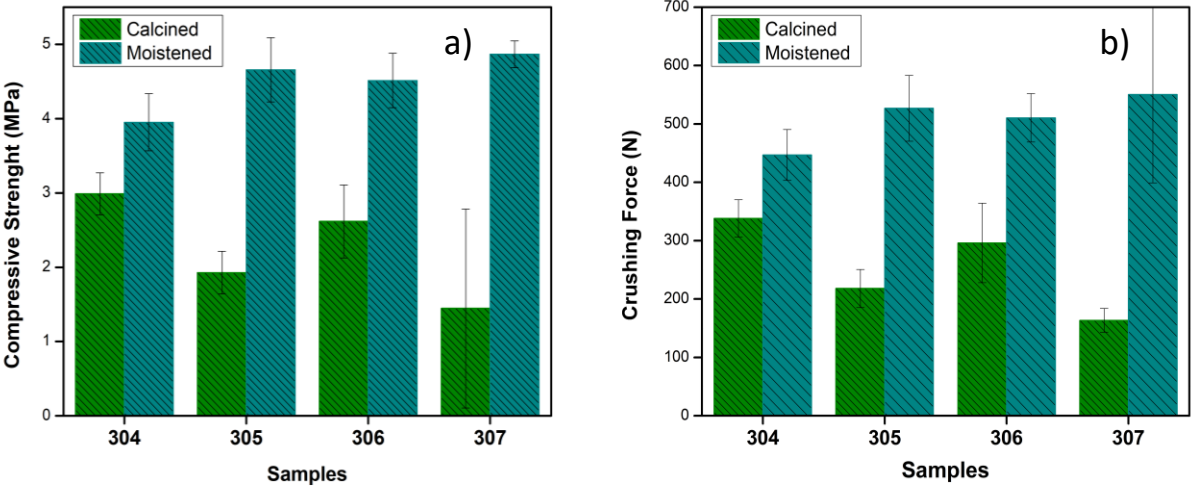
Figure 17 Compressive Strength and Crushing Force between calcined and moistened of CZY-304 sample.

6.1.3. Porosity test by volume differentiation

This method was used to observe total empty spaces, connected or not connected pores. Percentages between 22-31% porosity are shown in Table 6. This test shows results of a porosity on the order of microns.

Table 6 Data of dry and saturated clay after calcination process.

Sample	Dry weight (g)	Saturated weight (g)	Δweight (g)	%water	Δ%water
CZQ-306	4.2011	5.5211	1.32	31.4203	
	4.0438	5.3511	1.3073	32.3285	31.5297
	4.13	5.4037	1.2737	30.8402	
COL-307	4.4691	5.6924	1.2233	27.3724	
	4.5013	5.781	1.2797	28.4296	27.9565
	4.383	5.6132	1.2302	28.0675	
CZY-304	4.4097	5.518	1.1083	25.1332	
	4.499	5.6885	1.1895	26.4392	25.818
	4.4468	5.5977	1.1509	25.8815	
CZY-305	4.9878	6.0489	1.0611	21.2739	
	4.653	5.6987	1.0457	22.4737	22.0082
	4.6339	5.6662	1.0323	22.2771	

6.1.4. Porosity test by 3D nanotomography

The pore shape distribution showed in Figure 18 indicates the 3D-image of four samples, which host more spherical pores and blade-shaped pores. These pores are important due to they can store and transmit fluids through the connected pores[23]. In the left column 3D images are shown as a complete body and at the right column the 3D images has an orthogonal view that permits appreciate the pores. This technique helps to calculate porosity as a function of volume fractions. A preliminary visual scanning of the sample of the different samples reveals that most of the pore should be in the micro-scale.

Table 7 Results of 3D nanotomography of CZY-304 sample.

Description	Abbreviation	Value	Unit
Total VOI volume	TV	1.366E+12	um^3
Total VOI surface	TS	754080000	um^2
Closed porosity (percent)	Po(cl)	1.2975	%
Open porosity (percent)	Po(op)	0.155472369	%
Total porosity (percent)	Po(tot)	1.450800047	%
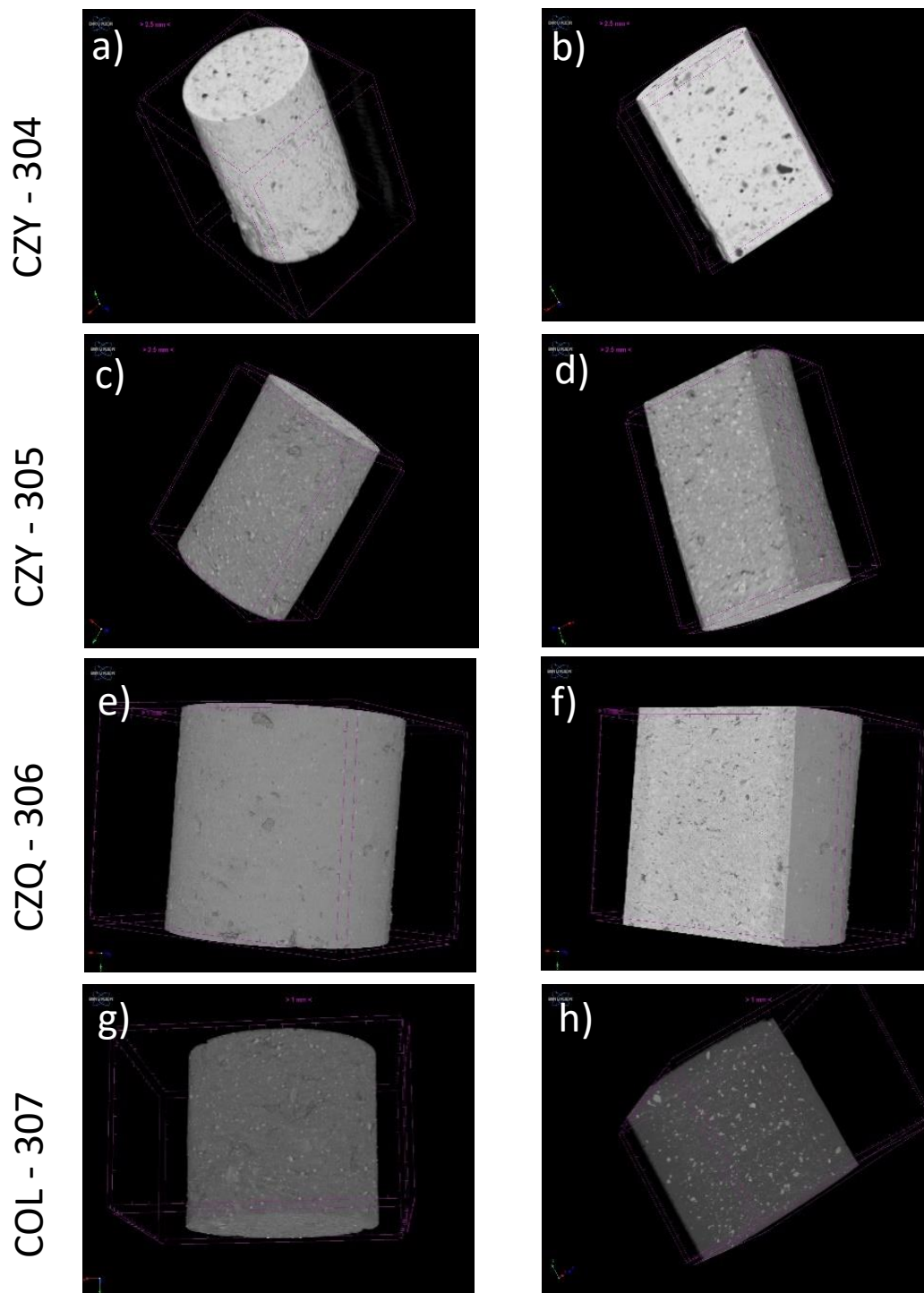
Figure 18 Nanotomography graphs of 3D samples (a,c,e,g) and longitudinal cuts (b,d,f,h) of calcined clays.

Figure 18 shows the 3D images of the four samples, but the table 7 just shows the results of the CZY-304 sample due that was the clay chosen for characterization and reactivity test.

After the mechanical tests carried out and the results obtained by the moistened clays, it was decided to continue only with calcined clays for the reactivity test, because the results found were contrary to the bibliography. But, in the same way, morphological characterizations were carried out for dry, calcined, and also for moistened clays to find their composition

6.2. . Dry and calcined clay characterization

6.2.1. Scanning Electron Microscopy - Electron Dispersive X-ray spectroscopy

The SEM image of the clay after the calcination process revealed a morphology in the form of small crystals superimposed on larger irregular shapes. The EDX spectrum of the boxed area indicates the presence of oxygen (O), silicon, (Si), aluminum (Al), phosphorus (P), Sodium (Na), nitrogen (N), and carbon (C) and the concentration results record in Figure 19.

Element Name	Atomic Concentration
Oxygen	64
Silicon	5.3
Aluminium	6.1
Phosphorus	1.3
Sodium	2.1
Nitrogen	9.6
Carbon	11.7
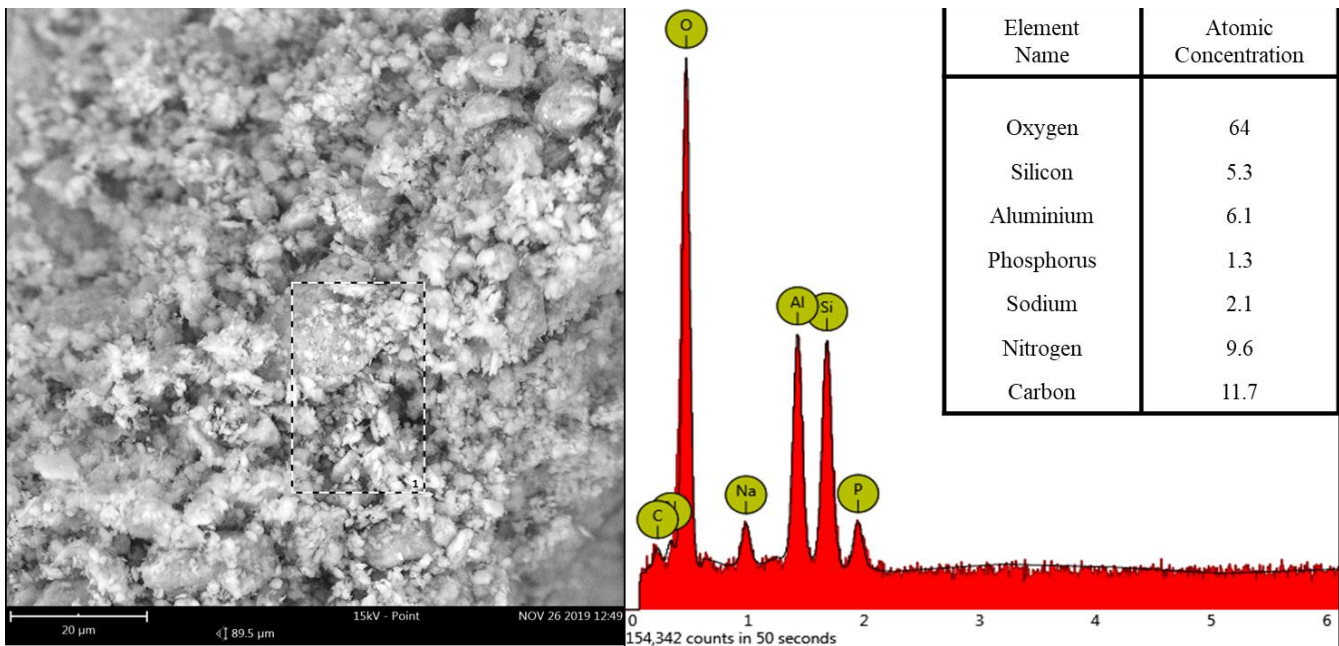
Figure 19 SEM-EDX results of CZY-304 calcined clay

6.2.2. Fourier-transform infrared spectroscopy

Transmittance spectrums of dry clays are showed in and described in Table 8. These results are divided in two regions. at intervals of 3800 cm^{-1} to 3500 cm^{-1} and 1400 cm^{-1} to 300 cm^{-1}. The objective is compare the functional groups after the calcination that took place at 450 °C for 14 hours, approximately.
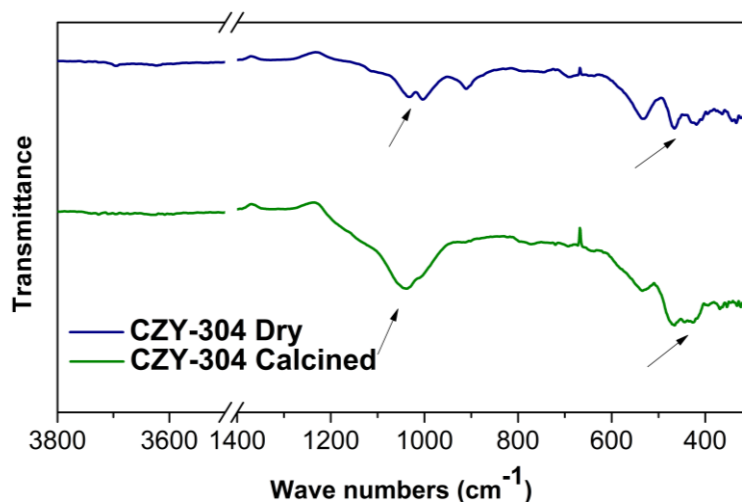
Figure 20 FTIR spectra of dry and calcined clay of CZY-304 sample.

Table 8 FT-IR data of dry and calcined clay of CZY-304 sample.

Peak Position Wavelength (cm^{-1})		Tentative Corresponding species
Dry	Calcined	
3695 VW	3693 VW	Hydroxyl groups (OH) of kaolinite
1032 W	1039 W	In-plane Si-O stretching
911 W	N/A	Al-OSi. of Illite and kaolinite
693 W	N/A	Si-O perpendicular
538 S	538 M	Al-O-Si deformation
466 M	468 M	Si-O-Si deformation
N/A	418 M	Si-O deformation

VS-Very Strong / M - Medium / S - Strong / W - Weak / VW - Very Weak

The 3695 cm^{-1} band had a very low intensity in all dry clay samples. This band represents the hydroxyl groups (OH) of kaolinite[24] and are totally absent in CZY-304 sample. this could represent or be an indicative of the disorder in the kaolinite's structure[25].

The Si-O stretching bands were found. In the studied kaolins, the vibrational assignments in the range of 909 - 914 cm^{-1} could be related with Al-OSi band. Perpendicular Si-O bands at 796 (medium band) and 787 (weak band) cm^{-1} respectively. Weak bands of Si-O were observed in CZY-304 sample at 693cm^{-1}. At the range of 533 – 420 cm^{-1} is founded different types of deformation bands as: Al-O-Si deformation. Si-O-Si deformation and Si-O deformation.

6.2.3. X-Ray Diffraction

The sample clay collected at 10Km South of Yanzatza canton, Zamora province was studied by XRD and results are show in Figure 21 and recorded in Table 11. Quartz is the main phase present with a 30% of relative abundance. The processed pattern displayed reflections of kaolinite, guidottite, feldspar and orthoclase (part of feldspar group) with ranges of relative abundance of 24-9 %. In less proportion muscovite, hematite, sernamontite, titanite, and zircon was present.
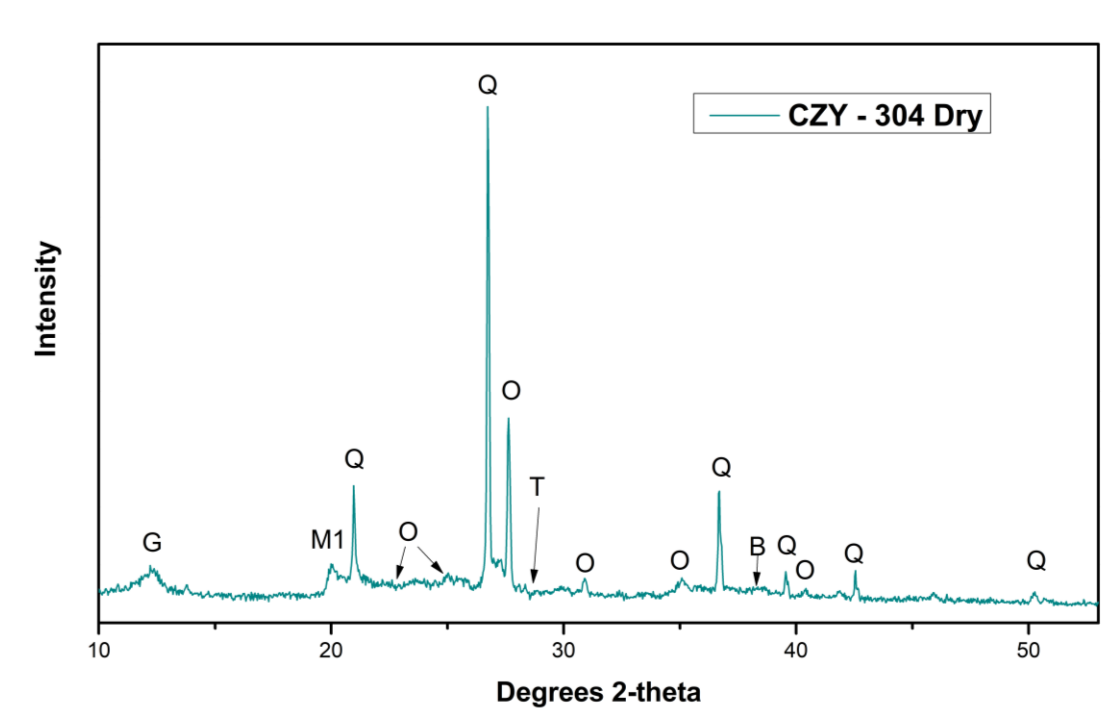
Figure 21 XRD dry clay of CZY-304 sample,

XRD patterns shows of calcined and dry samples showed small variations on the percentage of the relative abundance. So, calcined sample has the same compounds but with difference in the proportion. The mica mineral (muscovite) shows a 5.5% of relative abundance. Small amounts (<5%) of Brookite, sernamontite, zircon and feldspar were found. At 450 °C the amount of guidottite, zircon and feldspar decreased while the quantity of quartz, kaolinite, muscovite, orthoclase, and hematite among other increased.
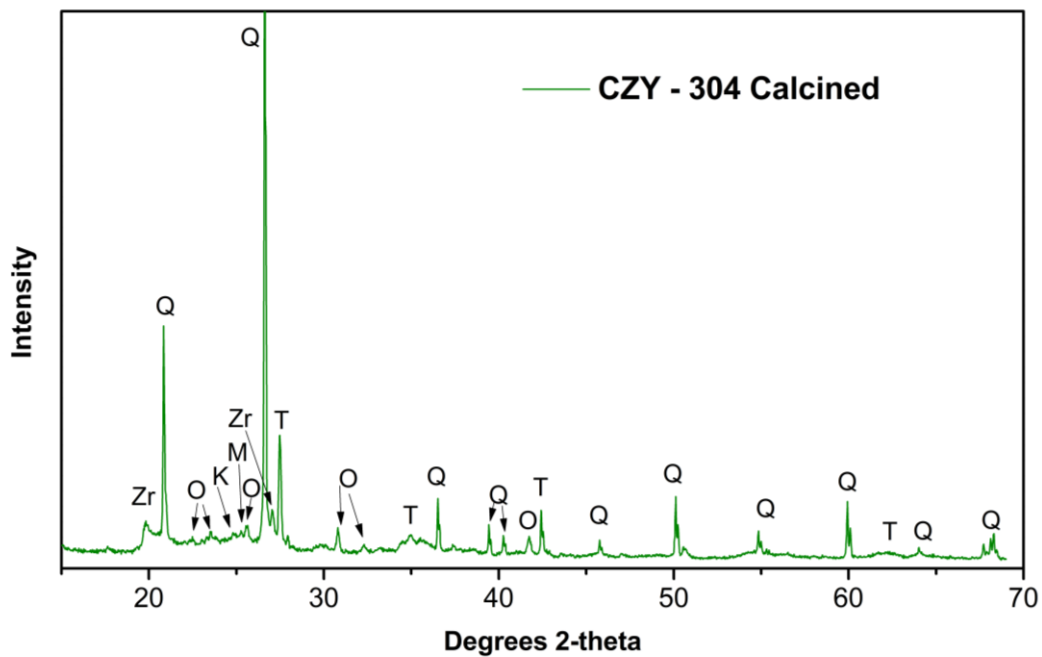
Figure 22 X-Ray Diffractogram of calcined sample
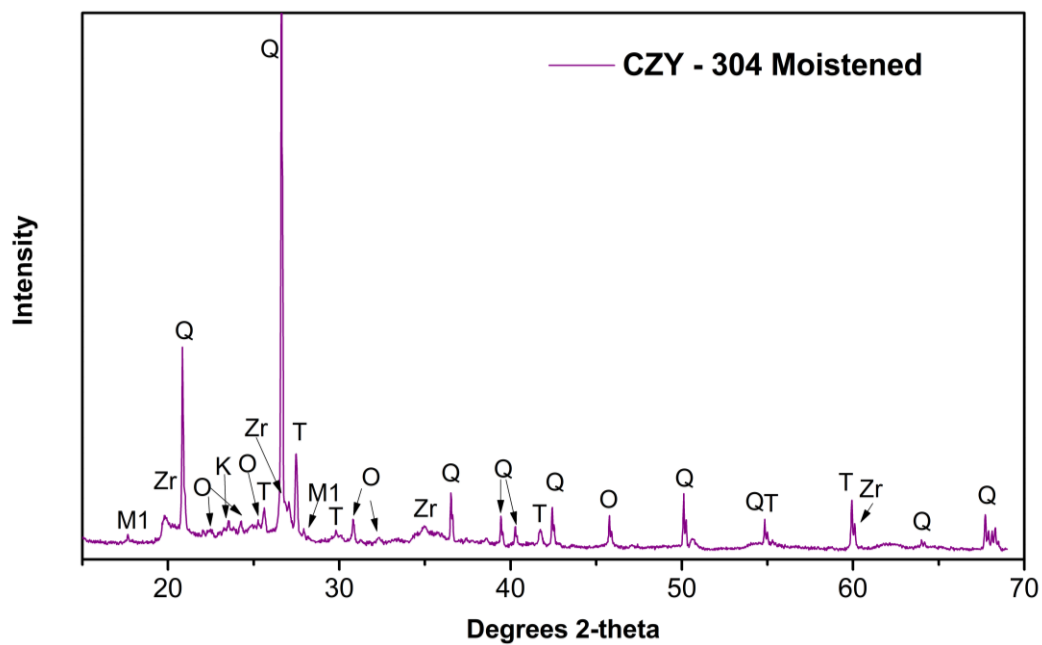
Figure 23 X-Ray Diffractogram of moistened sample

6.2.4. Thermal gravimetric analysis

The first objective of a good thermal analysis experiment is of course to separate optimally the successive steps of any thermal reaction. The conditions used in the measurements of the dry clays are: ramp speed of 10.00 °C/min. the sample gas is air, and the temperature range is 40-500 °C.

From the thermo gravimetrical curve, the sample size records 39.869 mg and exhibits a decomposition loss of 7.291 % weight (2.096 mg). The differential thermal analysis curve shows three main peaks, two sharp exothermic peaks at 47.53 °C and 474.41 °C and one exothermic peak at 251.31 °C. The first peak between ambient temperature and 150 °C represents de loss of water adsorbed on the surface of sheets and decomposition of organic products and represents the 1.957 % of percentage loss. The second peak is the loss of water of hydration, and the last peak usually associated with dehydroxylation of the clayey material. (See Figure 24)
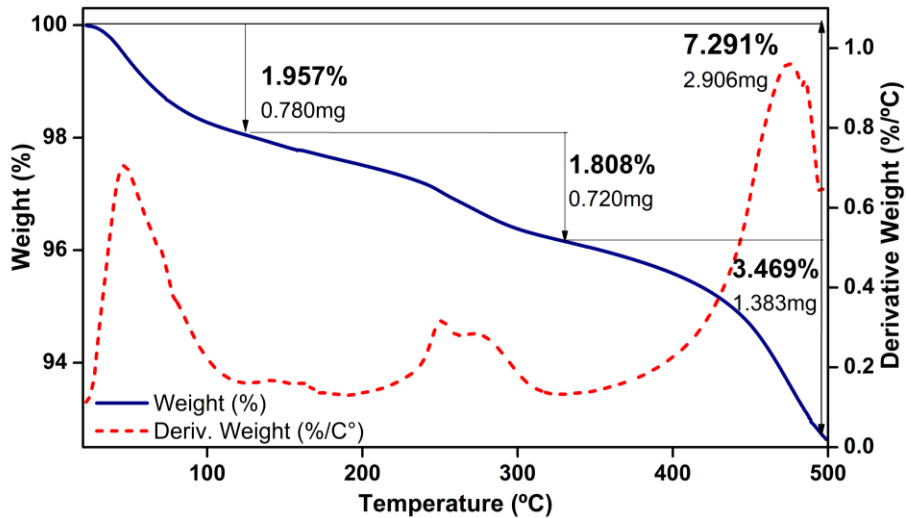
Figure 24 TGA (blue line) and DTG curve (red dash line) of CZY-304 sample.

The moistened clays lost 0.775 mg. which represents 2.222 % of total loss mass. (See Figure 25) From the DTG curve, there is a sharp exothermic peak at 43.40 °C, corresponding to the loss of physisorbed water. Comparing the moistened clay with the calcined one, both show the same sharp exothermic peak, but the moistened does not show the loss of water of hydration, which could be due to the transformation of the structure.
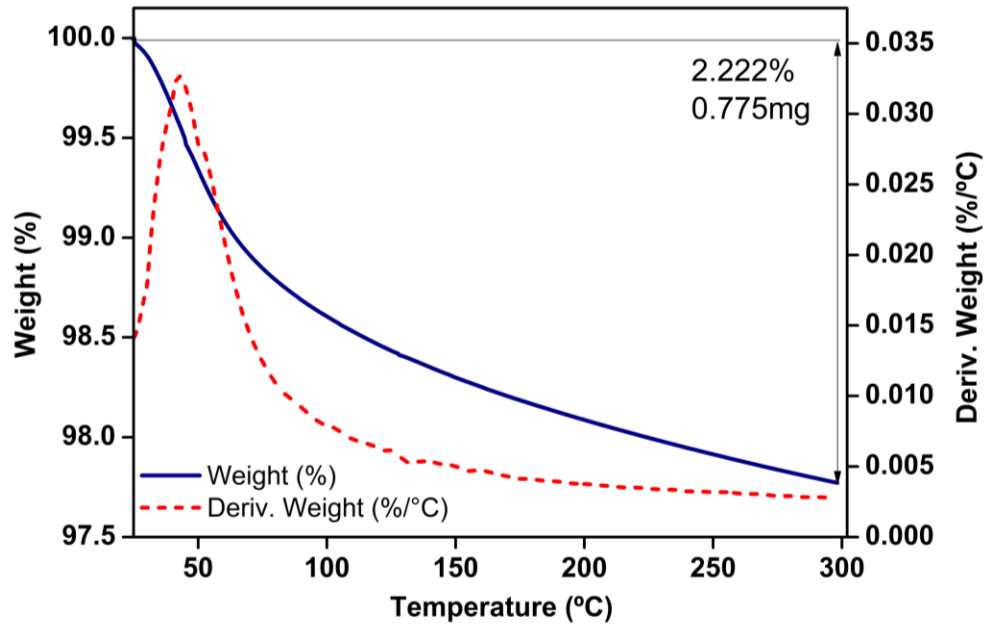
Figure 25 TGA - DTG diagram of CZY-304 moistened clay.

6.2.5. N$_2$ adsorption – desorption isotherms and mesopore analysis

The specific surface area was determined using the Brunauer-Emmett-Teller (BET) method. Fig 24 shows the N$_2$ adsorption-desorption isotherms of calcined and raw clay of CZY-304 sample. So according to the classification of the International Union of Pure and Applied Chemistry (IUPAC) both clays showed isotherms with a profile of type II, so this type is due to a characteristic material, which contains mesoporosity and has high energy of adsorption. This type of isotherm comes from an extra – structural pore spaces.
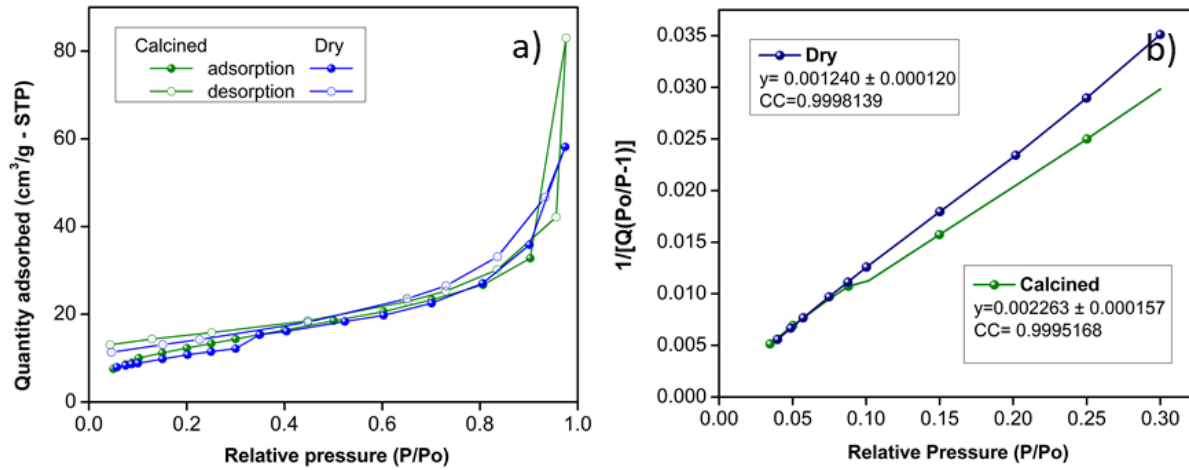
Figure 26 Comparison of calcined (green line) and dry (blue line) of clay sample at nitrogen adsorption (closed symbol) and desorption (open symbol) isotherms (a), and BET plot of the investigate clays (b).

Table 9 Results of BET and BJH analysis of calcined and raw sample.

Parameter	Raw	Calcined
Specific Area. S_{BET}	38.5112 m²/g	46.5426 m²/g
Correlation coefficient. R	0.9998139	0.9995168
External specific area. S_{ext}	40.7507 m²/g	57.3330 m²/g
Total pore volume. V_{BJH}	0.090908 cm³/g	0.130335 cm³/g
Adsorption average pore width	93.5396 Å	110.3588 Å

Total pore volume (V_{BJH}) and pore size distribution (PSD) was calculated using Barnett-Joyner-Halenda (BJH) procedure. Figure 27 shows total pore volume of dry and calcined clay with results of 93.5396 Å 110.3588 Å respectively, demonstrating increase in calcined clay.
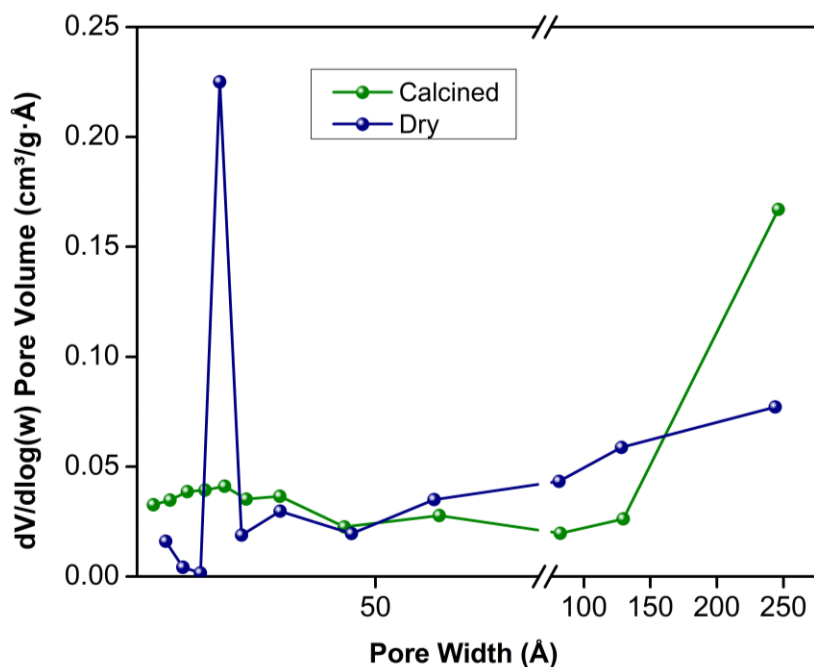
Figure 27 Comparison of pore size distribution between calcined (green line) and dry (blue line) CZY – 304 clay sample.

6.3. Reacted Clay Characterization
6.3.1. Visual analysis

After the reactivity test. the clay turns from a completely brown color to a mixture of colors that range from very light brown to green depending on the concentration of FeS in the reaction (See Figure 28). This visual analysis revealed that gas adsorption had been successful. From this point on, more test would be prepared to find out what elements had been adsorbed.
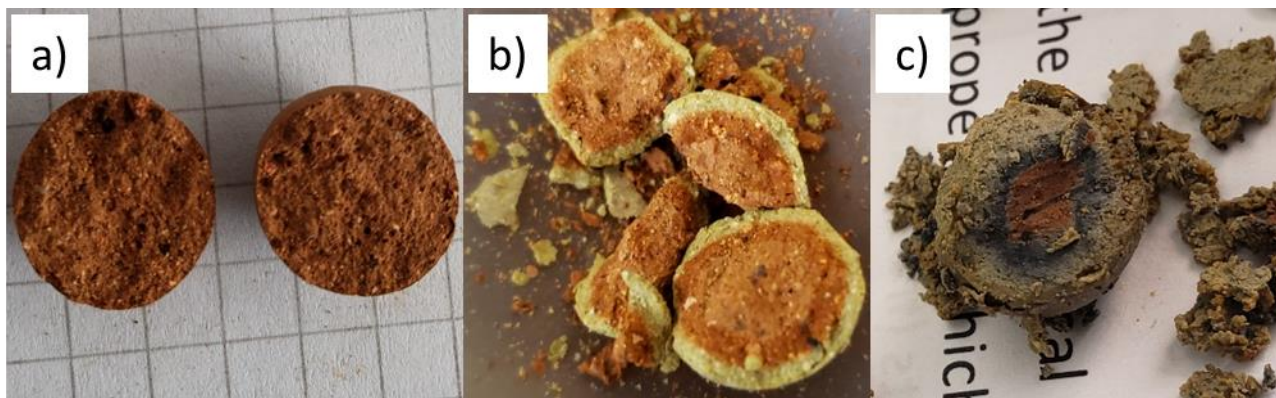
Figure 28 *Calcined (a) and reacted clays with 0.5 g (b) and 1.0 g (c) of FeS.*

6.3.2. Scanning Electron Microscopy –Energy Dispersive X-ray spectroscopy

The texture of the clay was rough and stiff, and its porosity was remarkable to the eye also from the visual test (See Figure 28). The presence of sulfur were expected in the clay samples reacted with different concentrations of ferrous sulfide. The SEM images of figures a) and c) showed the existence of luminous zones that were initially associated with sulfide. EDX spectrum of the area of the box in figure b) confirms the presence of sulfur with a 1.8% concentration as opposed to the 0.4 % concentration of sulfur present in the spectrum of the box in figure d). This 450 % increase in concentration between the clay reacted with 0.5 g. and 1.0 g of FeS confirms clay's ability to adsorb acid gases.
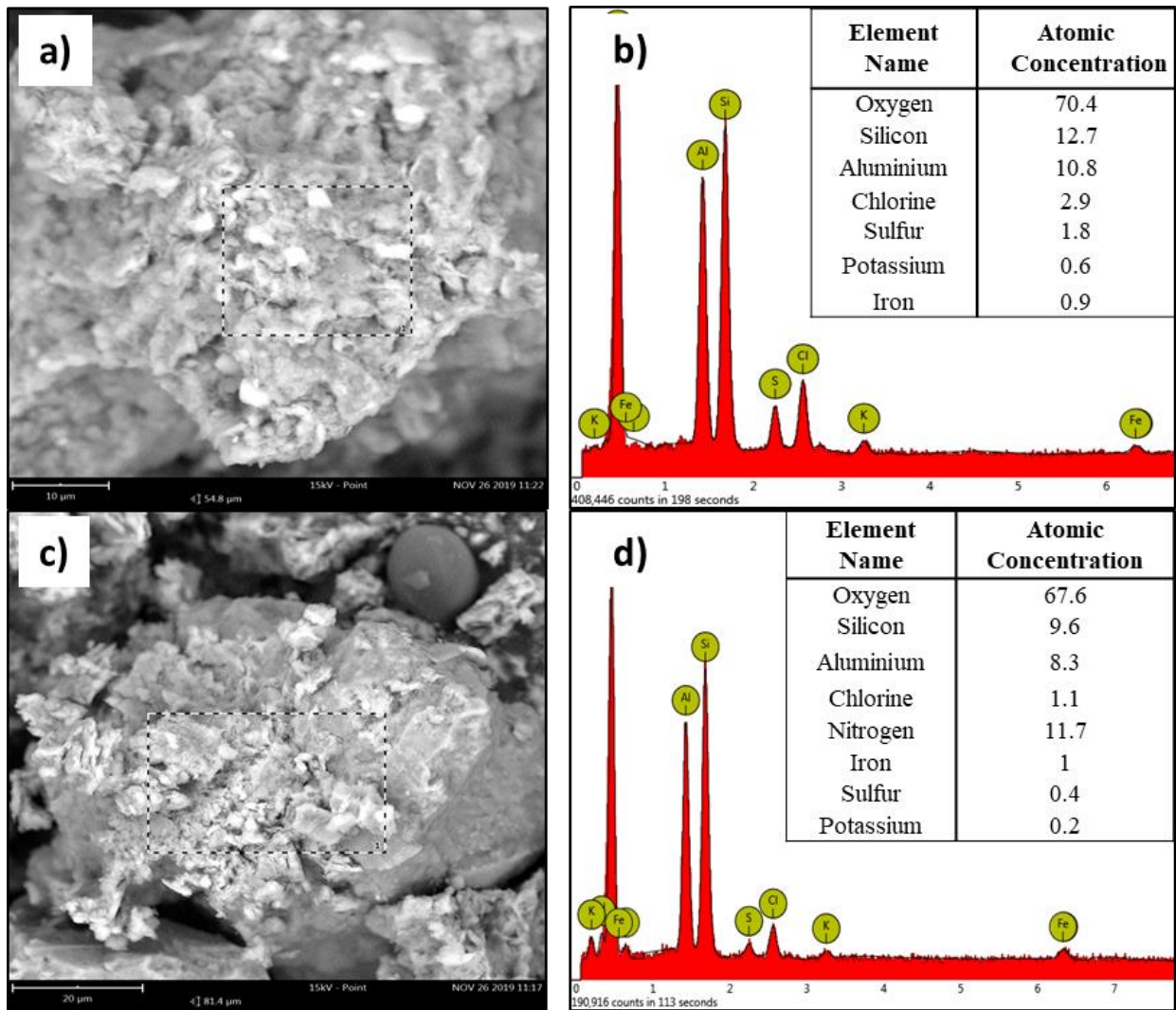
Figure 29 SEM-EDX analysis of reacted clays with (a), (b) 1.0 g. and (c), (d) with 0.5 g of FeS

6.3.3. X-ray Fluorescence spectroscopy

XRF characterization was performed to know the chemical composition of the minerals that are present in the clay. The Figure 30 shows the main differences in the low-energy region of the spectrum. These results spectra of the calcined and wet clay are the same and show elements such as: Ca, K, Ni, Sr, Ti, Zn and Zr. And the most notable results is the presence of Fe, Cl and S as it was expected. The presence of sulfur appears at an intensity of 26568 keV.
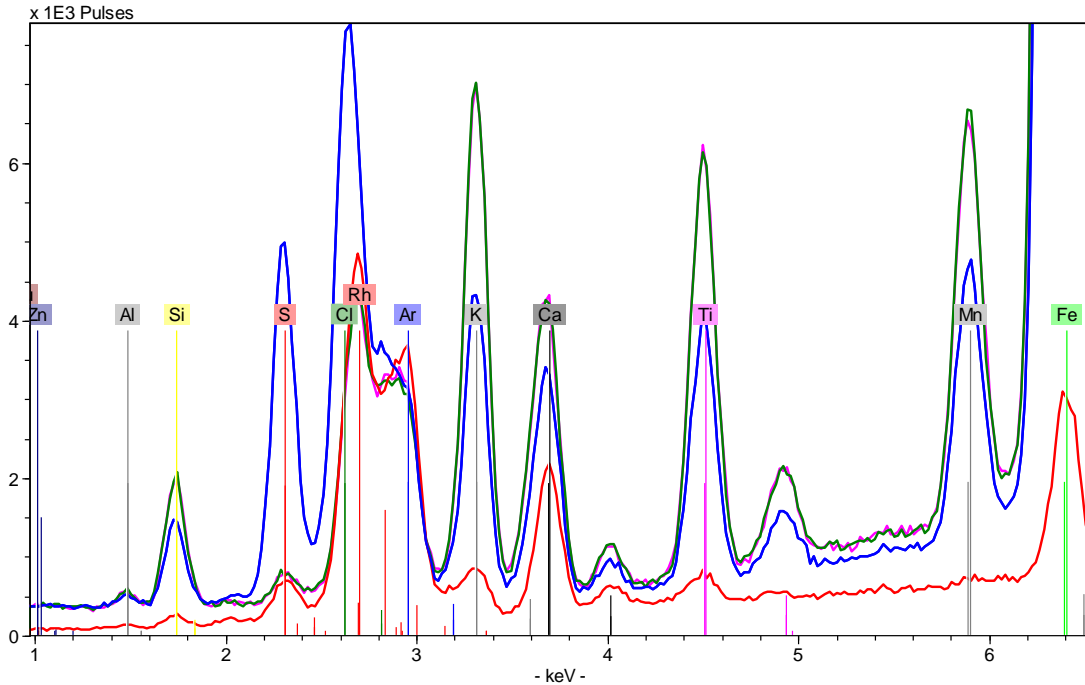
Figure 30 XRF spectrum of calcined (green), moistened (pink) and reacted (blue) clay sample.

Table 10 Net intensities of the XRF spectrums.

	Ca K$_{12}$	Cl K$_{12}$	Fe K$_{12}$	K K$_{12}$	Mn K$_{12}$	Ni K$_{12}$	S K$_{12}$	Sr K$_{12}$	Ti K$_{12}$	Zn K$_{12}$	Zr K$_{12}$
Blank	13543	7305	22183	2987	1904	8705	1888	128	3030	2428	186
Calcined	25193	3940	1379018	41998	48716	11459	1	7394	42233	7241	16122
Moistened	24863	3444	1383179	41777	48915	11754	1	7341	42859	7783	15205
Reacted	19043	33097	950455	23040	32936	12707	26568	6087	26428	6555	12313

These results are a guide to analyze the clays with the use of x-ray diffraction, knowing the elements that we must find in the crystalline phases.

6.3.4. X-Ray Diffraction

The XRD pattern of reacted clay sample showed in Figure 31 exhibited intense reflections of quartz (Q), which relative abundance was 24%. The diffractogram showed that quartz, kaolinite, guidottite, titanite and kornelite were the major phases present in the reacted sample. The presence of Kornelite (Ko), with a peak (210) at 13.23 Å, with a 13 % of relative abundance, which was absent in the XRD patterns of dry, calcined and moistened samples. This sulfate mineral has a monoclinic system. Sulfur detected fifteen peaks, (222) at 23.05 Å. Sulfur was detected by a peak (101) at 26.62 Å.
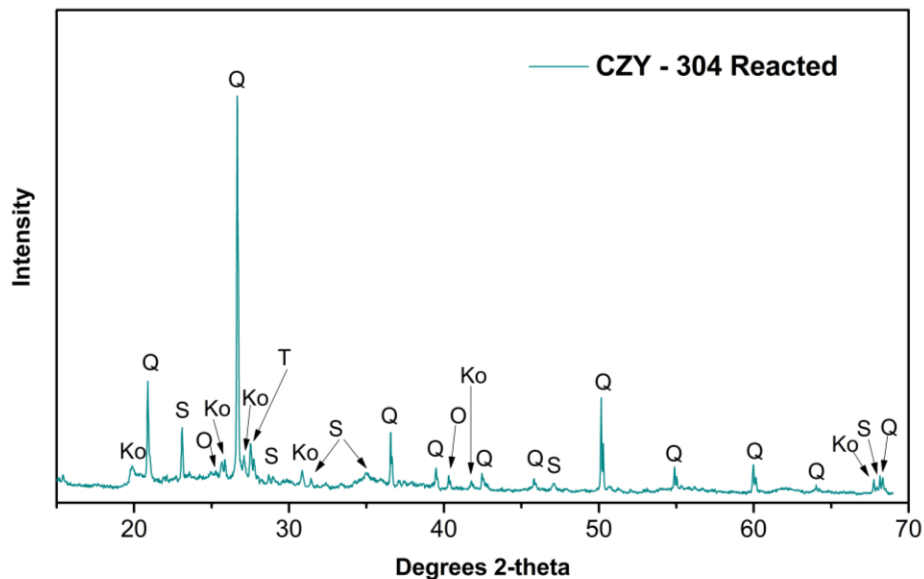
Figure 31 X-Ray Diffractogram of reacted clay of CZY-304 sample

Table 11 Quantitative analysis of dry, calcined, moistened and reacted clay of CZY-304 sample.

Compound Name	COD- CARD	Relative abundance (%)			
		Dry	Calcined	Moistened	Reacted
Quartz	00-101-1159	30	30.6	34.4	24
Kaolinite	00-900-9230	24	27.5	18	12.8
Guidottite	00-901-4441	10	6.5	7.2	9.8
Muscovite 2M1	00-101-1049	5	5.5	0.2	2.4
Brookite	00-900-4137	2.5	2.8	4.9	3
Hematite	00-900-4137	1.4	2.2	0.8	0.7
Orthoclase	00-210-8028	8	11.8	11.1	2.1
Sernamontite	00-1011201	4	1.1	0.3	0.3
Titanite	00-900-1327	0.4	4	1.4	11.6
Zircon	00-101-1261	3.4	1	1.8	6.6
Feldespar	00-900-3090	9	0.3	10.7	2.4
Sulfur	00-901-1362		-	-	6.8
Kornelite	00-900-0313		-	-	13

6.3.5. X-ray Photoelectron spectroscopy

The XPS results of the clay sample are typical of spectra of clay and clay minerals. The individual samples with their elemental percentages are presented in Figure 32. To evaluate the changes in chemical bonding the fitting curves of S 2p, O 1s, Si 2p, Al 2p and Fe 2p3, Cl 2p were studied.
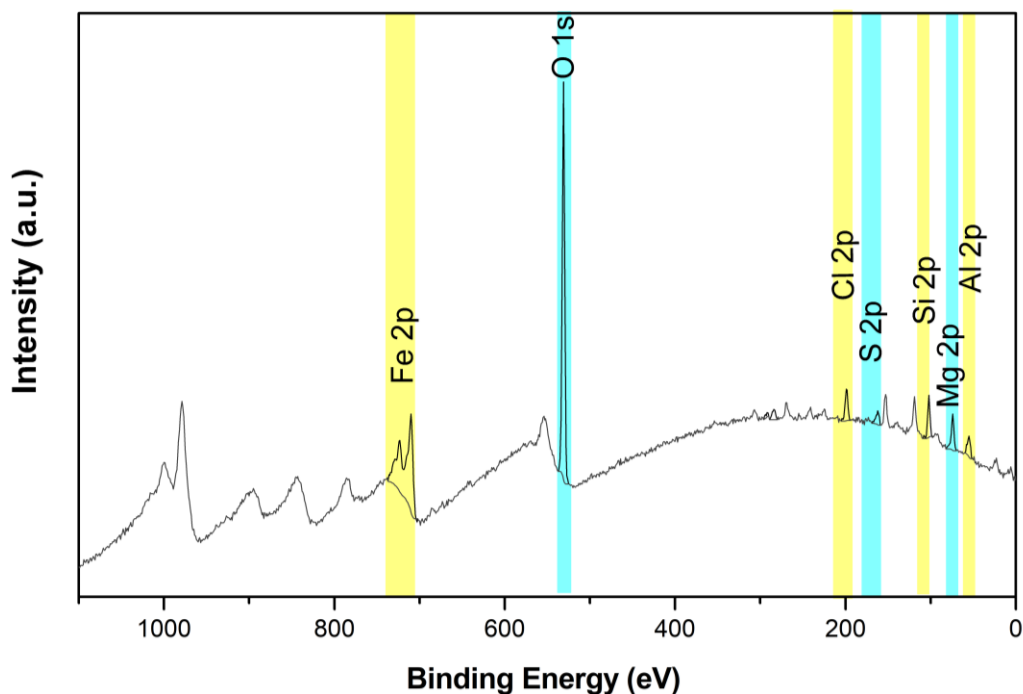
Figure 32 XPS Spectroscopy of CZY-304 clay sample.

The curve fitting results of the O1s and Si2p spectra (see Figure 33 e-f) show that the peaks at approximately 102.9 eV (SiO_2), and 103.8 eV (siloxane) for Si2p, and 531.0 eV, 532.3 eV and 533.3 eV for O1s are indications of the formation of the silicate network[26]. The O1s spectrum is strongly asymmetric and the transition observed at 532.2 eV is interpreted as belonging to iron (II) sulfate.
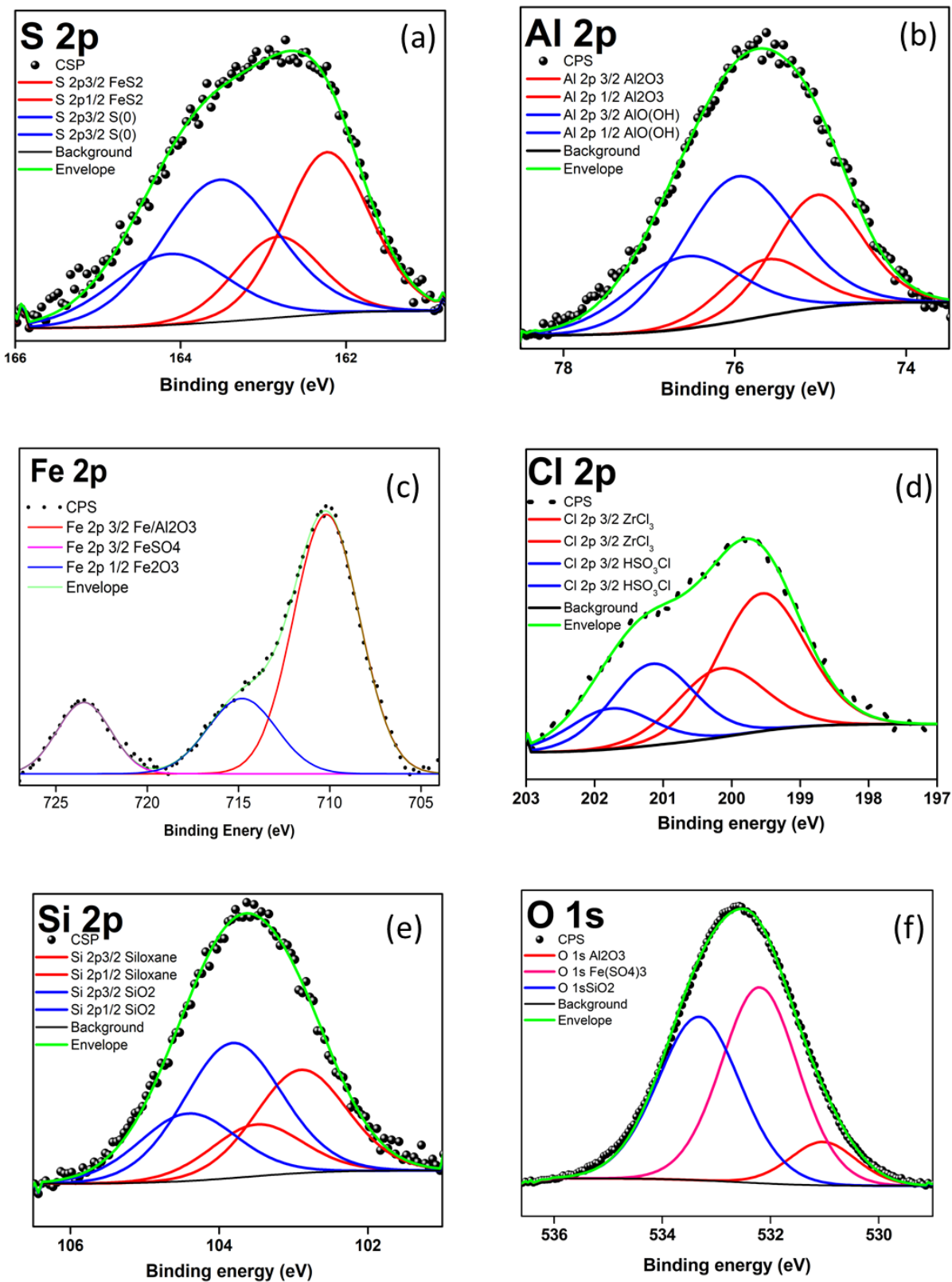
Figure 33 Fitting XPS spectra of S 2p (a), Al 2p (b), Fe 2p (c), Cl 2p (d), Si 2p (e), O 1s (f).

In kaolinite all aluminum are present in six-fold coordination in the octahedral sheets coordinated by oxygen atoms and hydroxyl groups[27] as it's confirmed in its curve fitting. The chlorine is observed as the Cl2p transitions around 199.6 eV and 201.2 eV. The Fe2p peak binding energies are at 709.9 eV, 714.24 eV and 723.36 eV and they are related to Fe-Al_2O_3, $FeSO_4$ and Fe_2O_3 respectively. Finally, the sulfur fitting curve showed the elemental sulfur that was found also with XRF spectroscopy, and XRD diffraction proving the adsorption of this element.

6.3.6. Reactivity

To test the pellet's clay as an adsorbent in gas streams in the capture hydrogen sulfide were used the reaction system described in section 5.4.1. This acid was generated through the exothermic reaction of iron (II) sulfide and excess of hydrochloric acid, creating:

$$FeS + HCl_{excess} \rightarrow H_2S + FeCl$$
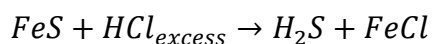
In this sense, in this work, the initial proposal was directed at the adsorption of hydrogen sulfide; however, the result obtained in the adsorption test yielded a conversion reaction of hydrogen sulfur conversion to elemental sulfur. So as shown in section 6.4.1, where the visual analysis showed at a reacted pellet's clay with different layers after the adsorption test, see Figure 28. The visual evaluation indicated the possible presence of elemental sulfur. Additionally, SEM-EDX, XRF, and XRD analysis confirmed it for the observation of crystals small of elemental sulfur, the sulfur's peak, and the crystalline phase of elemental sulfur as α-sulfur, respectively.

Figure 34 Clay after reactivity test, showing different color layers.

Therefore, the conversion reaction was not described as a fundamental concept of the scope of this work. Then, some aspects to understand it will be described.

Claus' reaction and oxidation of hydrogen sulfide

E. Alvarez et al.[28] studied the sulfur recovery from sour gas by using the low-temperature Claus process on sepiolite, which is a clay mineral. This work uses the catalytic reduction of sulfur dioxide by hydrogen sulfide through a reaction similar to the catalytic step of the Claus process:

$$2H_2S + SO_2 \rightleftharpoons \frac{3}{X}S_X + 2H_2O$$
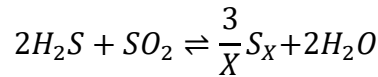
It is important to notice that the experimental set-up uses reactants as hydrogen sulfide and sulfur dioxide, unlike the reactivity process mentioned in section 5.4.1, where the experiment was not done in an inert environment, therefore there was the presence of air and carbon dioxide inside the balloon. Taking that into account, Herszae and Alfonso[29] showed the autooxidation of hydrogen sulfide in presence of Hematite and this reaction gives SO4, this result can be related with the apparition of Kornelite, $Fe_2(SO_4)_3$ 7H$_2$O, in the reacted diffractogram (See Figure 31), this behavior can be compared with the following equation:

$$4Fe_2O_3 + H_2S + 14H^+ \rightarrow 8Fe^{+2}_{aq} + SO_4^= + 8H_2O$$
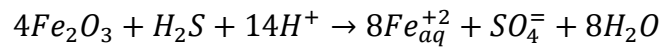
XPS fitting curves of Fe2p confirmed the presence of Fe_2O_3 and SO4 supporting the viability of the Clau's process. Also the XPS spectrum of S2p showed two chemical bonding, FeS$_2$ and elemental sulfur with peaks at 162.2 eV and 163.5 eV, respectively.

7. CHAPTER VII: CONCLUSSIONS AND RECOMMENDATIONS

7.1. CONCLUSSIONS

- Eight clays were collected from southern part of Ecuador, at three provinces, Azuay, Zamora Chinchipe and Morona Santiago and all of them were dry and then calcined.

- Creation of special molds to recreate equal pellets in form of spheres and cylinders depending the purpose and requisites of the test.

- Free-fall drop test was successfully done, according to Tavares and Almeida the drop number for a good pellet should be at least four, therefore CZY – 304, CZY – 305, CZQ – 306 and COL – 307 resist more than the minimum of falls. In this test, the CZY – 304 clay sample records an average of eight drops until the rupture.

- Porosity was determined using the volumetric differentiation and 3D nanotomography, with a range of percentages between 22 – 31 %. 3D images gives a clear image of the pore size distribution.

- Strength compression and Force was suitable to choose the best clay for further investigation. After these mechanical test, CZY – 304 clay sample was chosen due to good results on uniaxial compression.

- From this point, all the results are for CZY – 304 sample.

- Scanning Electron Microscopy – Energy Dispersive X-Ray (SEM-EDX) revealed the presence of oxygen (O), silicon, (Si), aluminum (Al), phosphorus (P), Sodium (Na), nitrogen (N), and carbon (C) on dry clay sample. For reacted sample, the same elements were found with a difference of the sulfur presence, which reveal 0.4 % of atomic concentration when the clay was reacted with 0.5 g of FeS and when it is reacted with 1.0 g the atomic concentration increases until 1.8 %.

- Fourier Transformed Infrared Spectroscopy (FTIR) showed peaks in the ranges of 1400 cm^{-1} to 300 cm^{-1}, with these results the presence of disordered kaolinite can be proved. Dry and calcined clays shows the same peaks with small differences.

- X-Ray Diffraction (XRD) shows the presence of quartz, kaolinite, guidottite, orthoclase, muscovite, hematite, sernamontite, titanite, and zircon at dry and calcined sample. The results obtained in both diffractograms showed that the dominant clay mineral was kaolinite.

- Thermal gravimetric analysis (TGA) determined the mass loss up to 500 °C, the mass loss were due to water of hydration, and with dehydroxylation of the clayey material.

- Calcined and dry clays showed isotherms with a profile similar to type II isotherm, so this type is due to a characteristic material, which contains mesoporosity and has high energy of adsorption.

- X-Ray Fluorescence spectroscopy helped to find out the elemental composition in order to investigate more with XRD diffractograms. The presence of Ca, K, Ni, Sr, Ti, Zn and Zr was in dry, calcined and reacted clay. But in reacted clay the appearance of sulfur was confirmed.

- X-ray powder diffraction technique analyze the mineralogical composition of the clays and revealed the presence of quartz, kaolinite, guidottite, muscovite, brookite, hematite, orthoclase, sernamontite, titanite, zircon and feldspar. For reacted sample, a new clay mineral was found, Kornelite, besides that, sulfur was founded with a 6.8 % of relative abundance.

- X-ray Photoelectron spectroscopy determine chemical environment, Fe2p fitting curve confirmed the existence of SO_4.

7.2. RECOMMENDATIONS

For TGA/DTG successful experimental practice, it is appropriate to consider:

- Dry materials should be of high purity.

- Fine -grained powder should be used to achieve greater contact area and better equilibrium conditions.

- The time at any temperature must be sufficiently long in order to permit completeness of reactions.

- The weight sample should be in the range of 30 – 60 mg. and it is better if all the samples weight approximately the same.

Bibliography

1. San Sebastián M, Hurtig AK. Oil exploitation in the Amazon basin of Ecuador: A public health emergency. *Rev Panam Salud Publica/Pan Am J Public Heal*. 2004;15(3):205-211. doi:10.1590/S1020-49892004000300014

2. Haard D. *Oil and Gas Production Handbook: An Introduction to Oil and Gas Production*.; 2006. doi:10.1016/S1359-0294(00)00069-8

3. Shah MS, Tsapatsis M, Siepmann JI. Hydrogen Sulfide Capture: From Absorption in Polar Liquids to Oxide, Zeolite, and Metal-Organic Framework Adsorbents and Membranes. *Chem Rev*. 2017;117(14):9755-9803. doi:10.1021/acs.chemrev.7b00095

4. Sudamerica OW. Ecuador - Country Analysis Briefs. 2011;(September):1-6. http://www.oilwatchsudamerica.org/doc/eia_ecuador.pdf.

5. Banco Central del Ecuador. Reporte Del Sector. 2019:31.

6. Al-janabi YT. An Overview of Corrosion in Oil and Gas Industry: Upstream, Midstream and Downstream Sectors. *Corrossion Inhib Oil Gas Ind*. 2020:1-39. doi:10.1002/9783527822140

7. Uribe RA. Investigaciones de Materias Primas Minerales No Metálicas en el Ecuador. *Rev Politécnica*. 2015;36(3):34-44. http://revistapolitecnica.epn.edu.ec/ojs2/index.php/revista_politecnica2/article/view/607.

8. Guidotti TL. Occupational exposure to hydrogen sulfide in the sour gas industry: some unresolved issues. *Int Arch Occup Environ Health*. 1994;66(3):153-160. doi:10.1007/BF00380773

9. Occupational Safety and Health Administration. OSHA FactSheet - Hydrogen Sulfide (H2S). 2005:2. https://www.osha.gov/OshDoc/data_Hurricane_Facts/hydrogen_sulfide_fact.pdf.

10. Skrtic L. Hydrogen Sulfide, Oil and Gas, and People's Health. *Energy*. 2006;(May):1-77. http://www.fe.doe.gov/programs/gasregulation/authorizations/2011_applications/exhibits_ 11-161-LNG/39_Skrtic_Report.pdf.

11.   Jiang J, Chan A, Ali S, et al. Hydrogen Sulfide-Mechanisms of Toxicity and Development of an Antidote. *Sci Rep*. 2016;6(January):1-10. doi:10.1038/srep20831

12.   Guidotti TL. Hydrogen sulfide: Advances in understanding human toxicity. *Int J Toxicol*. 2010;29(6):569-581. doi:10.1177/1091581810384882

13.   Hsu YY, Yu CC. A Self-Learning Fault Diagnosis System Based on Reinforcement Learning. *Ind Eng Chem Res*. 1992;31(8):1937-1946. doi:10.1021/ie00008a015

14.   Liu Y, King HE, van Huis MA, Drury MR, Plümper O. Nano-tomography of porous geological materials using focused ion beam-scanning electron microscopy. *Minerals*. 2016;6(4). doi:10.3390/min6040104

15.   Software C, Capabilities SOF. CT-analyser and CT-volume. C:2-3.

16.   Altomare A, Corriero N, Cuocci C, Falcicchio A, Moliterni A, Rizzi R. QUALX2.0: A qualitative phase analysis software using the freely available database POW-COD. *J Appl Crystallogr*. 2015;48:598-603. doi:10.1107/S1600576715002319

17.   SmartLab Guidance Reference Manual.

18.   Graulis S, Chateigner D, Downs RT, et al. Crystallography Open Database - An open-access collection of crystal structures. *J Appl Crystallogr*. 2009;42(4):726-729. doi:10.1107/S0021889809016690

19.   Merkys A, Vaitkus A, Butkus J, Okulič-Kazarinas M, Kairys V, Gražulis S. COD::CIF::Parser: An error-correcting CIF parser for the Perl language. *J Appl Crystallogr*. 2016;49:292-301. doi:10.1107/S1600576715022396

20.   Hanawalt JD. Manual Search/Match Methods For Powder Diffraction in 1986. *Powder Diffr*. 1986;1(1):7-13. doi:10.1017/S0885715600011209

21.   Advances in X-Ray Analysis, Vol. 37, Edited by J.V. CJilfridi el al.. Plenum Press, New York, 1994 37. 1994;37:37-47.

22.   Toraya H. Whole-powder-pattern fitting without reference to a structural model: application to X-ray powder diffraction data. *J Appl Crystallogr*. 1986;19(6):440-447. doi:10.1107/s0021889886088982

23. Kong L, Ostadhassan M, Li C, Tamimi N. Pore characterization of 3D-printed gypsum rocks: a comprehensive approach. *J Mater Sci*. 2018;53(7):5063-5078. doi:10.1007/s10853-017-1953-1

24. GRIM RE. Properties of Clay. *Recent Mar Sediments*. 1955:466-495. doi:10.2110/pec.55.04.0466

25. Bukalo NN, Ekosse GIE, Odiyo JO, Ogola JS. Fourier Transform Infrared Spectroscopy of Clay Size Fraction of Cretaceous-Tertiary Kaolins in the Douala Sub-Basin, Cameroon. *Open Geosci*. 2017;9(1):407-418. doi:10.1515/geo-2017-0031

26. Wang W, Tian G, Zong L, et al. From illite/smectite clay to mesoporous silicate adsorbent for efficient removal of chlortetracycline from water. *J Environ Sci (China)*. 2017;51:31-43. doi:10.1016/j.jes.2016.09.008

27. Kloprogge, J.T., Wood BJ. Baseline studies of the Clay Minerals Society Source Clays by X-ray Photoelectron Spectroscopy. *Clay Sci*. 2018;22(4):85-94. doi:10.11362/jcssjclayscience.22.4

28. Alvarez E, Mendioroz S, Muñoz V, Palacios JM. Sulphur recovery from sour gas by using a modified low-temperature Claus process on sepiolite. *Appl Catal B Environ*. 1996;9(1-4):179-199. doi:10.1016/0926-3373(96)90080-6

29. Herszage J, Dos Santos Afonso M. The autooxidation of hydrogen sulfide in the presence of hematite. *Colloids Surfaces A Physicochem Eng Asp*. 2000;168(1):61-69. doi:10.1016/S0927-7757(99)00453-7

30. Ul-Hamid A. *A Beginners' Guide to Scanning Electron Microscopy*.; 2018. doi:10.1007/978-3-319-98482-7

31. Rouquerol F, Rouquerol J, Llewellyn P. *Chapter 2.12 – Thermal Analysis*. Vol 5. 2nd ed. Elsevier Ltd.; 2013. doi:10.1016/B978-0-08-098259-5.00014-7

32. Ayres P. A beginner's guide to Twitter. *ALISS Q*. 2009;v. 4, no.4:6-9.

33. در الله, سیروس،چوبینه. *No Title*□□□□: □□□□□ □□□□ □□□□□□□□□□ □□□□ 1389.;)□□□ □□□(□□□□ □□□□□□□□□.

34.   Brouwer P. *Theory of XRF*.; 2010.

35.   Wagner CD, Riggs WM, Davis LE, Moulder JF, Muilenberg GE. Handbook of X-ray electron spectroscopy. *Perkin-Elmer Corp*. 1979:192.

36.   Chukanov N V., Chervonnyi AD. *Infrared Spectroscopy of Minerals and Related Compounds*.; 2016. doi:10.1007/978-3-319-25349-7

37.   Amelinckx S. Electron Diffraction and Transmission Electron Microscopy. *Mater Sci Technol*. 2006. doi:10.1002/9783527603978.mst0010

38.   Pansu M, Gautheyrou J. *Chapter 26: Cation Exchange Capacity*.; 2006. doi:10.1007/978-3-540-31211-6_26

ANNEX

Characterization methods of mineral clays

The particle size, elemental composition, mineralogical composition of clays are analyzed with many characterization techniques.

Microscopy analysis

The scanning electron microscope (SEM) is uniquely suited for studying clays because it affords a magnified, three-dimensional view of the unmodified (natural) clay surface with great depth of focus. This technique shows the interaction between the electrons and the matter, as this technique works without visible light the images ends on white and black. The electron beam necessary for the operation of the SEM is produced and controlled within the microscope column. This column includes the electron gun for generating the electron beam and two or more electron lenses. The column is operated under vacuum and provides accelerating voltages in the range of 0.5 kV to 40 kV in commercially available instruments.

The images are obtained by scanning an electron beam of high energy on the sample surface. hence the name scanning electron microscope. By virtue of its smaller wavelength. electrons are able to resolve finer features/details of materials to a much greater extent compared with optical light. A modern day SEM can magnify objects up to one million times their original size and can resolve features smaller than 1 nm in dimension.[30]

Micro-determinations are usually carried out by X-ray fluorescence spectrometry by means of an EDX spectrometer. This system enables plotting of charts of elementary qualitative distribution at the surface layer and on approximately 1 µm thickness. It is better to use almost flat surfaces; for accurate quantitative analysis. surfaces have to be polished to 0.25 µm to limit possible topographical effects[31].

Thermal Analysis

Thermal analysis, in general, can be defined as a general method embracing any technique where a physical property of the sample is recorded versus the temperature, is a measurable property such as mass, temperature difference, length, flow of evolved gas, etc.

Thermogravimetric Analysis is a technique in which the mass of a substance is monitored as a function of temperature or time as the sample specimen is subjected to a controlled temperature program in a controlled atmosphere. A TGA consists of a sample pan that is supported by a precision balance. That pan resides in a furnace and is heated or cooled during the experiment. The mass of the sample is monitored during the experiment. A sample purge gas controls the sample environment. This gas may be inert or a reactive gas that flows over the sample and exits through an exhaust. The latter limitation is overcome by thermogravimetry (TG), where the quantity measured is the sample mass. Here, the mass of water evolved is precisely measured, whatever its type of bonding to the clay mineral. Another advantage of TG is the possibility to select slow heating rates. Which, contrary to DTA or DSC. do not lower the sensitivity or accuracy of the experiment[32].

A DSC analyzer measures the energy changes that occur as a sample is heated, cooled or held isothermally, together with the temperature at which these changes occur. The energy changes enable the user to find and measure the transitions that occur in the sample quantitatively, and to note the temperature where they occur, and so to characterize a material for melting processes, measurement of glass transitions and a range of more complex A Practical Introduction to Differential Scanning Calorimetry 3 events. One of the big advantages of DSC is that samples are very easily encapsulated, usually with little or no preparation, ready to be placed in the DSC. so that measurements can be quickly and easily made[33].

Nitrogen adsorption - desorption Analysis

BET analysis provides precise specific surface area evaluation of materials by nitrogen multilayer adsorption measured as a function of relative pressure using a fully automated analyzer. The technique encompasses external area and pore area evaluations to determine the total specific surface area in m2/g. yielding important information in studying the effects of surface porosity and particle size in many applications.

BJH analysis can also be employed to determine pore area and specific pore volume using adsorption and desorption techniques. This technique characterizes pore size distribution independent of external area due to particle size of the sample.

X-Ray powder diffraction

X-ray diffraction has acted as the cornerstone of twentieth century science. Its development has catalyzed the developments of all of the rest of solid state science and much of our understanding of chemical bonding. This article presents all of the necessary background to understand the applications of X-ray analysis to materials science. The applications of X-rays to materials characterization will be emphasized, with particular attention to the modern, computer assisted, approach to these methods.

Spectroscopy analysis

X-ray fluorescence (XRF) spectroscopy is an analytical method to determine the chemical composition of all kinds of materials. The materials can be in solid, liquid, powder, filtered or other form, XRF can also sometimes be used to determine the thickness and composition of layers and coatings.

The method is fast, accurate and non-destructive, and usually requires only a minimum of sample preparation. Applications are very broad and include the metal, cement, oil, polymer, plastic and food industries, along with mining, mineralogy and geology, and environmental analysis of water and waste materials[34].

Surface analysis by ESCA involves irradiation of the solid in vacuo with monoenergetic soft x-rays and sorting the emitted electros by energy. The spectrum obtained is a plot of the number of emitted electrons per energy interval versus their kinetic energy. Each element has a unique elemental spectrum. and the spectral peaks from a mixture are approximately the sum of the elemental peaks from the individual constituents. Since the mean free path of the electrons is very small. the electrons which are detected originate from only the top few atomic layers. Quantitative data can be obtained from the peak heights or areas and identification of chemical states often can be made from the exact positions and separations of the peaks. as well as from certain spectral contours[35].

FTIR

Absorption bands observed in the IR spectrum of a crystalline compound are the result of the resonant interaction of radiation with collective vibrations of a large number of atoms. However, with a certain degree of approximation IR bands in different frequency ranges can be associated with vibrations of appropriate groups of atoms[36]

X-Ray Diffraction (XRD)

X-rays are relatively short wavelength, high energy electromagnetic radiation. When viewed as a wave we think of it as a sinusoidal oscillating electric field with, at right angles, a similar varying magnetic field changing with time. The other description is that of a particle of energy called a photon. All electromagnetic radiation is characterized by either its energy E. wavelength k (i.e.. the distance between peaks) or its frequency v (the number of peaks which pass a point per second). The following are useful relationships for interconverting the most common measures of radiation energy.

$$\lambda = \frac{c}{v}$$

$$E = hv$$

where c is the speed of light and h is Planck's constant. Spectroscopists commonly use wavenumbers particularly in the low energy regions of the electromagnetic spectrum, like the microwave and infrared. A wave number (v) is frequency divided by the speed of light

$$\bar{v} = \frac{v}{c} = \frac{c/\lambda}{c} = \frac{1}{\lambda}$$

The angstrom (A) unit. defined as 1 x 10"10 m. is the most common unit of measure for X-rays but the last IUPAC vention made the nanometer (1 x 10~9m) a standard. However, here we will use the traditional angstrom unit. Energy in electron volts (eV) is related to angstroms through the formula.

$$E(eV) = \frac{hc}{\lambda_{cm}} = \frac{12396}{\lambda_{Å}}$$

Electron volts are also not IUPAC approved in that the standard energy unit is the Joule which may be converted by

$$1eV = 1.602 \ x \ 10^{-19}J$$

It should be noted that despite the IUPAC convention. Joules are never used by crystallographers or spectroscopists. while a few workers have adopted the nanometer in place of the angstrom[37].

Certain minerals can be "amorphous" to X-ray either because they do not have a specific crystalline arrangement (true of glasses) or because they have short-range organization that is too small to be detected at a wavelength of 1–2 Å. XRD is not the best technique for the study of non-crystalline solids such as allophanes which are made up of clusters of Si atoms presenting structural elements with interlayer distances corresponding to 1 or 2 neighbouring atoms[38].